ENCAPSULATION OF GASES IN ZEOLITE 3A

AND

TEMPERATURE PROGRAMMED DESORPTION

OF THE TRAPPED GASES

ENCAPSULATION OF GASES IN ZEOLITE 3A AND TEMPERATURE PROGRAMMED DESORPTION OF THE TRAPPED GASES

by

Yun-cheung Chan, B. Eng.

A Thesis

Submitted to the Faculty of Graduate Studies

in Partial Fulfilment of the Requirements

for the Degree

Master of Engineering

McMaster University

October, 1976

MASTER OF ENGINEERING (Chemical Engineering) — McMASTER UNIVERSITY, Hamilton, Ontario

TITLE: Encapsulation of Gases in Zeolite 3A and Temperature Programmed Desorption of the Trapped Gases

AUTHOR: Yun-cheung Chan, B. Eng. (McMaster University)

SUPERVISOR: Professor R.B. Anderson

NUMBER OF PAGES: ix, 112

SCOPE AND CONTENTS:

Gases (Ar, N_2 and CO_2) were encapsulated in zeolite 3A at high temperature (350°C) and pressure (maximum pressure obtained from a gas cylinder). Temperature programmed desorption (TPD), with a linear temperature schedule, was applied to study the kinetics of the release of the trapped gases. The TPD spectra for argon show two peaks (a large peak at about 350°C and a small one at about 500°C, for a heating rate of 17°C per minute) and there is only one peak in the spectra for nitrogen and carbon dioxide. The spectra obtained were analysed using a diffusion equation (Fick's Second Law of diffusion) taking into account the shape and size distribution of the particles. The effect of water addition was shown to enhance the rate of desorption of the trapped gases.

ACKNOWLEDGEMENTS

The author would like to thank those people who have rendered their assistance in this work.

I wish to express my special thanks to Dr. Robert B. Anderson, my research supervisor, for his patience and encouragement.

I am grateful to Dr. C. Gillies, Dr. J. Zielinski, Mr. C. Machiels and especially Mr. C.B. Lee for their helpful discussions.

The financial support received from McMaster University is sincerely acknowledged.

Y. C. Chan

Hamilton, Oct., 1976

TABLE OF CONTENTS

LIST OF TABLES

LIST OF FIGURES

CHAPTER 1

INTRODUCTION

1.1 Introduction

Molecular sieve zeolites are crystalline aluminosilicates with pores of uniform size which are uniquely determined by the structure of the crystal. These naturally occurring minerals have long been recognized as selective adsorbents and the application was limited to dessicants prior to 1950. Not all zeolitic minerals are good adsorbents; the structure of some zeolites (e.g. heulandite, stilbite) collapse on dehydration at 300°C. Only those thermally stable to dehydration are of value. The difficulty of identifying and characterizing the structure of the product hindered the development of synthetic zeolites in the early decades (1,2). Commercial manufacture of synthetic zeolite was initiated after the success of producing the new synthetic zeolite A in 1956 by Reed and Breck of Union Carbide Corporation. At present synthetic zeolites have found many industrial applications. Among these are separation and recovery of normal paraffin hydrocarbons, catalysis of hydrocarbon reactions, drying of refrigerants, separation of air components, etc.

If the zeolite is evacuated at 350°C to remove the water molecules that occupy the pores and then exposed to a gas or vapour, the high internal surface area and void space in the zeolite will adsorb rapidly until it is saturated. However, the adsorption of gases may be selective due to the

molecular sieve action made possible by the intracrystalline pores of molecular dimensions. The diffusion of one species into the solid may be totally prevented while the diffusion of a second species takes place. In some cases, partial molecular sieve action may occur; components of mixtures may diffuse into the solids at different rates depending upon the conditions. When the gas molecule has a diameter approaching that of the pore opening, the interaction between the cation and the gas molecule is energetically significant. If the aperture is sufficiently small relative to the size of the diffusing molecule, then repulsive interactions become dominant. The energy required for the molecule to pass through the aperture is the activation for diffusion, E, as expressed by the Arrhenius equation (3),

$$D = D_0 \exp(-E/RT)$$

Apart from the steric effect imposed by the size of diffusing molecules and that of the pore opening, the magnitude of interaction between the cations and gas molecules depends on the polarizing power of the cations and the electronic nature of the gas molecules. The polarizing ability (charge/radius) increases as the cation size decreases because of the higher concentration of positive charge (4). Thus, zeolite 4A with the cation radius of Na of 0.95 Å has a stronger polarizing power than 3A with the radius of K^+ equal to 1.33 Å. This property tends to decrease diffusivities of molecules by decreasing their mobilities through specific interaction with the cation. Polar molecules and molecules with π bonds or un-

bonded electrons have high affinities for zeolites, but have lower diffusivities than molecules of comparable size not having these electrical properties (5).

For potassium-exchanged Type A zeolite (3A), the size of the pore openings is about 3 Å. At normal adsorption temperature and pressure only molecules with an effective diameter less than 3 Å (e.g. H_2 , He, H_2O and NH_3) are small enough to be adsorbed. However, larger molecules may permeate the crystal at high temperature and pressure. If the crystals are allowed to cool to room temperature slowly and the pressure subsequently reduced, they may contain sizable amounts of gas that is trapped or encapsulated.

The trapping of gases in molecular sieves with molecular diameters greater than the pore openings of the molecular sieves may provide a means for the storage of gas. This is possible because of the extremely low diffusivities of gases from the sieve at room temperature. The energy barrier has to be overcome in order to discharge the trapped gas. When energy barriers E are low (less than 15 kcal/mole) crystals charged with the gas tend to leak at room temperature. If the energy barriers are high, the guest molecules are released only at high temperatures.

Temperature programmed desorption has been used to study the active sites of catalysts (6). For gases chemisorbed on energetically different sites several maxima (peaks) may appear on the desorption spectrum since different activation energies are required for desorption of gas molecules from

energetically different sites. One of the advantages of the method is that control of the initial amount of gases released is achieved so that accurate analysis of data is possible. By monitoring the heating rate, the number of different sites may be obtained. In a single experiment, a relatively short time will be required to deplete the adsorbed gas in the sample compared with those desorption experiments conducted under constant temperature.

1.2 Structure of Type A Zeolite

The structure of zeolites (7) consists of a three-dimensional framework of SiO_4 and AlO_4 tetrahedra, usually simple arrangements of polyhedron. Each polyhedron itself is a three-dimensional array of silica-alumina tetrahedra in a definite geometric form. For type A zeolites , the basic sodalite group has the tetrahedra arranged at corners of a truncated octahedra and these octahedra are linked in a cubic array by joining them with cubes on the square faces (Fig.1.1). The cavity thus formed is called the α-cage with a free diameter of 11.4 Å that is entered through six circular apertures formed by a nearly regular ring of eight oxygen atoms with a free diameter of 4.2 Å. These cavities give rise to a system of unduloid-like channels with a maximum diameter of 11 Å and minimum of 4.2 Å. The truncated octahedra themselves enclose a second set of cavities, each having a free diameter of 6.6 Å (β-cage). These smaller cavities are connected to the larger cavities by means of a distorted ring of six oxygen atoms of 2.2 Å free diameter (Fig. 1.2).

The unit cell of zeolite A contains 24 tetrahedra, 12 AlO_4 and 12 SiO_4 , and 27 water molecules when fully hydrated. Normally zeolite A is synthesized in the Na-form. The chemical formula is

$$Na_{12}\{(AlO_2)_{12}(SiO_2)_{12}\}27\ H_2O$$

Other cationic forms are prepared by ion exchange in aqueous solution. The potassium-exchanged form is

Figure 1.1 Type A Zeolite Structure

(a) SODALITE CAGE

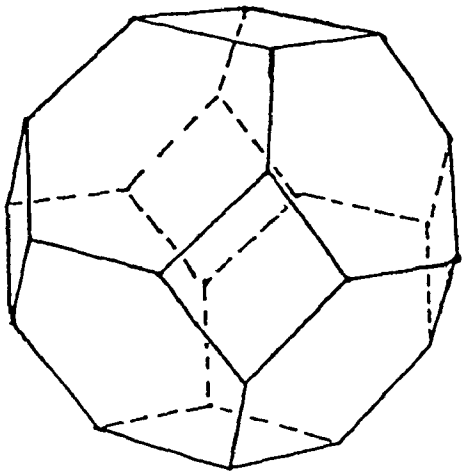

(b) CUBIC ARRAY

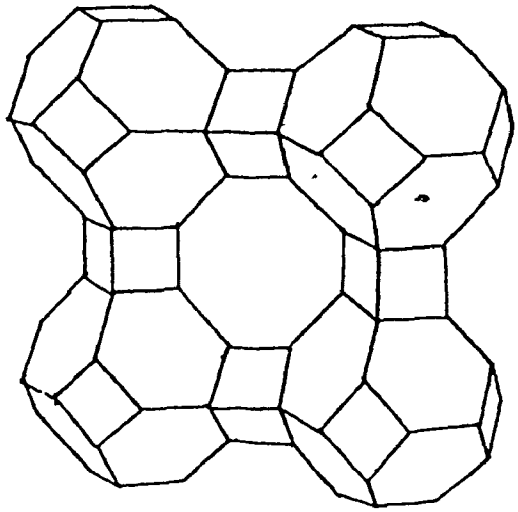

Fig.1.2

A diagram of the (110) section of zeolite A illustrating the relative positions and dimensions of the α-cages and β-cages. • Na^+ in site I.

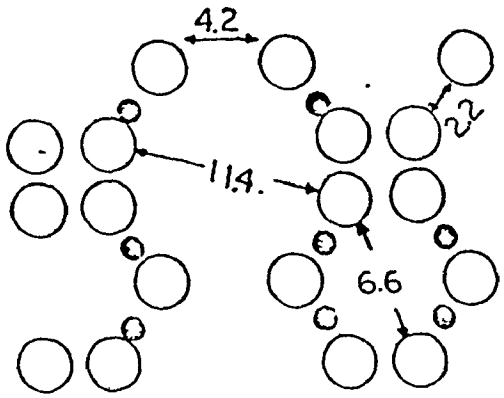

$$K_{12}\{(AlO_2)_{12}(SiO_2)_{12}\}\,24\ H_2O$$

When dehydrated the unit cell constant of KA decreases by 0.008 Å, thus confirming the very rigid nature of the aluminosilicate framework. The smaller number of H_2O molecules in KA is due to the larger size of K^+.

In the hydrated structure, 8 Na^+ are located near the centre of the 6-oxygen-membered rings on the 3-fold axis inside the α-cage. This position is referred to as site I. The remaining 4 Na^+ appear to be located with water molecules in the 8-rings.

In the dehydrated structure, 8 Na^+ (Na_I) are displaced 0.4 Å into the α-cage from the centre of the 6-rings. 3 Na^+ (Na_{II}) are located in the 8-rings displaced about 1.2 Å from the centre (8). The Na_{II} cations, by partial blocking of the aperture, influence the adsorption of gases and vapors and determine the size of the pore opening. The remaining sodium ion has been located opposite the 4-ring.

In potassium-exchanged zeolite A, K^+ ions in site II restrict the free opening of the 8-rings so that molecules with diameters greater than 3 Å are excluded. The K^+ positions in KA are likely to be similar, except for the effect of ionic radius, to those of the Na^+ ions in NaA (9). In Ca^{++}exchanged A, there are 4 Ca^{++} and 4 Na^+. The 8 site I positions are occupied and the site II positions are vacant. The apertures are completely open and capable of admitting molecules with diameters of about 4.3 Å.

1.3 Literature Review

1.3.1 Encapsulation

Encapsulation of inert gases in heulandite, stilbite, tridymite, cristobalite, sodalite and crancrinite (10,11,12) were studied by Barrer and his coworkers. Samples were prepared in stainless steel capsules. The gases were pressurized using an Aminco hydraulic high pressure pump coupled to a Sprague 200 cubic inches intensifier unit. Some degree of lattice collapse was reported at high pressure and temperature. Fick's Law solution for spherical particles was used to interpret the desorption kinetics. The expression of the diffusivity at temperature T for short time was shown to be

$$D(T) = \frac{\pi}{4A^2}\frac{dZ}{dt}^2$$

where A is the surface area per unit volume of the crystalline phase, Z is the fraction of the gas desorbed from the sample. The diffusion coefficients D(T) were found from the initial linear portion of the graph of Z versus $\sqrt{t}$. Table 1.1 shows some of the diffusivities data.

Data for the encapsulation of CH_4, C_2H_4, Ar and Kr in zeolite 3A were given by Breck (13) at pressures up to 4300 atmospheres and a temperature of 350°C. However, no diffusivity data were given. The amount of argon encapsulated at 2650 atmospheres and 350°C was 109 c.c.(S.T.P.)/g and only 77 c.c.(S.T.P.)/g remained after 79 days at room temperature. For the case of Kr the amount of gas trapped at 4300 atm. and 350°C remained constant for 30 days. This may indicate that

permanant trapping of larger molecules inside the cages of 3A sieve at room temperature. Table 1.2 gives the results for other gases.

Nelson and Walker (14) reported diffusivities data for Ar and N_2 in zeolite 3A measured in a differential system. The method consisted of charging the sample under investigation at low pressures and constant temperature (about 1.4 atm. and 300°C), and then measuring the release of gas after a sudden decrease of the pressure to atmospheric. The total volume of gas that could be loaded into a given sample is small. Fick's Law solution at constant temperature was used to determine the diffusion coefficients. The results are shown in Table 1.3.

In a series of publications Grant and Carter (15,16) discussed ion trapping and gas release phenomena. Fick's diffusion equation was solved for the case of an initially planar distribution of migrating species, located at a specific depth below the surface of a semi-infinite medium, whilst the medium was subjected to a heating schedule of the form $(1/T) = (1/T_0) - \alpha t$, where α is a constant. It was shown that the rate of species migrating across the surface boundary increases to a maximum at a specific temperature and then decreases with further heating. The temperature of the maximum is related to the activation energy for diffusion, the initial depth of the migrating species and the heating rate.

Table 1.1 Diffusion Coefficients ($D = D_o \exp(-E/RT)$) for Inert Gases in Heulandite, Stilbite, Tridymite, Cristobalite, Sodalite and Cancrinite. (10,11,12)

Sorbent	Temp. Range (^oK)	Diffusivities (cm^2 / sec.)			
		He	Ar	Ne	Kr
Heulandite	297-440	-	$3.4 \times 10^{-5} \exp(-15500/RT)$	$1.66 \times 10^{-8} \exp(-2900/RT)$	-
Stilbite	423-492	-	$5.6 \times 10^{-8} \exp(-8200/RT)$	-	$1.0 \times 10^{-6} \exp(-1200/RT)$
α-tridymite	235-335	$7.7 \times 10^{-4} \exp(-12000/RT)$	-	$6.7 \times 10^{-2} \exp(-22500/RT)$	-
β-tridymite	418-474	-	-	$9.9 \times 10^{-1} \exp(-24100/RT)$	-
α-cristobalite	244-335	$2.0 \times 10^{-2} \exp(-13800/RT)$	-	$2.0 \times 10^{-2} \exp(-13800/RT)$	-
Sodalite	485-602	-	$3.3 \times 10^{-4} \exp(-30000/RT)$	-	$1.1 \exp(-52000/RT)$
Cancrinite	587-633	-	$1.6 \times 10^{12} \exp(-71000/RT)$	-	-

TABLE 1.2

Encapsulation of gases in Zeolite 3A (13)

Gas	Kinetic Diameter (σ Å)	Encapsulation Temp. (°C)	Encapsulation Pressure (Atm.)	Amount Trapped After t days at 25°C. (c.c.STP/g)
CH_4	3.8	350	2650	105, t = 4
				98 , t = 37
C_2H_4	3.9	250	830	81, t = 2
				76, t = 35
Ar	3.4	350	2650	109, t = 3
				77, t = 79
Kr	3.6	350	4300	90.5, t = 1
				90.5, t = 30

TABLE 1.3

Rate Parameters for Ar and N_2

Diffusing Through Zeolite 3A (14)

Gas	Temperature Range (°C)	$D_o^{\frac{1}{2}}/r_o$ ($sec.^{-\frac{1}{2}}$)	E (kcal/mole)
Ar	280 - 400	6.2	14.0
N_2	293 - 363	15.8	16.2

1.3.2 Temperature Programmed Desorption Techniques

Cvetanovic and Amenomiya (6) gave a very good introduction to the experimental techniques as well as theoretical considerations of the desorption process. Based on first order desorption kinetics, the authors derived equations for linear temperature increase relating the peak temperature (T_m) and the heating rate (α) in terms of activation energy of desorption (E) and the pre-exponential factor (A) :

1) Case 1 - No readsorption

$$-\log \alpha = E/(2.21RT_m) + \log (278R/AE)$$

2) Case 2 - Readsorption

$$-\log \alpha = H/(2.21RT_m) + \log (278R(1-\theta)^2 v/HA'F)$$

3) Case 3 - Diffusion controlled

$$-\log \alpha = H/(2.19RT_m) + \log((R/H)^{1.5}(1150L^2/A'D_o^{2}))$$

where H is the heat of desorption, θ is the coverage at T_m, R is the gas constant and D_o is the pre-exponential factor of the diffusion coefficient. The slopes of the plots of $-\log \alpha$ versus $1/T_m$ differ negligibly for case 3 from the first two cases. This seems to indicate that there is no significant difference between the activation energy for desorption and the activation energy for diffusion. However, the authors omitted all except the first term of the series of the Fick's Law solution. This approximation holds only near the end of the desorption. In this range the rate has first order kinetics.

A detailed analysis of the desorption controlled process was given by Smutek, Cerny and Buzek (17). A general case of desorption kinetics of order x was considered. Three different temperature schedules were applied (linear, exponential and hyperbolic). The conditions at peak temperature were given as

$$\frac{xkT_m \exp(-\varepsilon)}{\alpha_z \cdot \varepsilon} = (1/\theta)^{x-1}$$

where x = order of desorption

k = rate constant for desorption

T_m = peak temperature

θ = surface coverage at T_m

$\varepsilon = E/RT_m$

α_z = heating rate

$= \alpha . T_m^{2-z}$ where z = 0,1,2 stand for hyperbolic, exponential and linear schedules respectively.

1.3.3 Factors Affecting Sorption Rates

The preadsorption of polar molecules such as water, ammonia drastically reduced the capacity for adsorption of gases in mordenite and chabazite (18,19). It is believed that the blocking action of the polar molecules effectively seals off portions of the zeolite crystals. In fact some inconsistent diffusivity data were due to the residual water molecules that were present before adsorption because of the incomplete dehydration of the zeolite at 350°C. A temperature of 400°C was recommended to evacuate the sample in vacuo (20).

The concentration dependence of diffusivity complicates the evaluation of diffusivities of gases in zeolites. Ruthven and Loughlin (21) avoided this problem by using relatively small changes in sorbate concentration so that the diffusivity at a particular concentration could be evaluated. Eagan and Anderson (22) evaluated diffusivities at the last 20 % of the rate curve. It was shown that the diffusivity approaches a constant value as equilibrium is reached. This diffusivity was assigned to the equilibrium concentration. Diffusivities calculated by this method also eliminated the temperature effect that distorts the rate curve at the start of the experiment. A difference of about 20 % in diffusivity results if the first 80 % of the rate curve were employed.

Ruthven and Loughlin (21) showed that both the shape and size distribution of the zeolite crystallites

have significant effects on the sorption curves. A normal distribution (on a weight basis) was used to modify the solution of Fick's Law of diffusion. A weight average particle size was shown by Eagan and Anderson (22) to be adequate for interpreting the data. Based on particle size distribution, a rate curve was calculated in terms of Dt/a_v^2 , where a_v is the weight mean particle size. This calculated curve was compared with the experimental data by plotting Dt/a_v^2 as a function of t for different values of Z. The plot was shown to follow a straight line for the value of Dt/a^2 larger than .14 .

CHAPTER 2

DESORPTION KINETICS

2.1 Fick's Law Solutions

Fick's Second Law of diffusion has often been used to interpret kinetic data for diffusion controlled processes. If the desorption of encapsulated gas is diffusion controlled, then Fick's Law may be adequate to describe the process. Consider first of all, a spherical particle of radius a for illustrative purpose. Solutions for other geometries will be given subsequently (Table 3.1). Assuming uniform initial concentration throughout the particle and constant diffusivity D (independent of concentration), the solution of Fick's Second Law of diffusion

$$\frac{\partial u}{\partial t} = D\frac{\partial^2 u}{\partial r^2} \qquad (1)$$

with initial condition, $u = rC_o$ at $t = 0$

and boundary conditions: u is bounded at $r = 0$

$u = 0$ at $r = a$

where $u = rC$, r = distance from centre of the sphere and C is the concentration, is given by Crank (23).

The fraction of diffusing substance leaving the sphere is

$$Z = 1 - (6/\pi^2)\sum_{n=1}^{\infty}\frac{1}{n^2}\exp(-Dn^2\pi^2 t/a^2) \qquad (2)$$

where n is an integer. An alternate solution is

$$Z = 6(Dt/a^2)^{1/2}\left[\frac{1}{\sqrt{\pi}} + 2\sum_{n=1}^{\infty} \text{ierfc}(na/(Dt)^{1/2})\right] - 3Dt/a^2 \qquad (3)$$

For the case of variable temperature, if D is related to the temperature T by the Arrhenius equation $D = D_o \exp(-E/RT)$, equation (1) becomes

$$\frac{\partial u}{\partial \tau'} = \frac{\partial^2 u}{\partial r^2} \tag{4}$$

where $\tau' = \int_o^t D\, dt$ (5)

The solution to equation (4) is in the same form as equation (2) and (3) except the term Dt is replaced by τ'. Putting $\tau = \tau'/a^2$, we have

$$Z = 6\tau^{\frac{1}{2}}(\pi^{-\frac{1}{2}} + 2\sum_{n=1}^{\infty} \text{ierf}(n\tau^{-\frac{1}{2}})) - 3\tau \tag{6}$$

and $$Z = 1 - (6/\pi^2)\sum_{n=1}^{\infty} \frac{1}{n^2} \exp(-n^2\pi^2\tau) \tag{7}$$

Note that equation (6) converges well for small time because for $\tau < .16$, the series $\sum_{n=1}^{\infty} \text{ierf}(n\tau^{-\frac{1}{2}})$ is equal to zero. Thus, for $\tau < .16$,

$$Z = 6(\tau/\pi)^{\frac{1}{2}} - 3\tau \tag{8}$$

Also equation (7) converges well for long time so that for $\tau > .16$,

$$Z = 1 - (6/\pi^2)\exp(-\pi^2\tau) \tag{9}$$

Equation (8) can be rearranged in the form

$$(\pi\tau)^{\frac{1}{2}} = 1 \pm (1 - \pi Z/3)^{\frac{1}{2}}$$

The negative sign of the square root is chosen by noting that as $Z \to 0, \tau \to 0$. Differentiating (8) with respect to time gives

$$\frac{dZ}{dt} = 3(\pi\tau)^{\frac{1}{2}} \frac{d\tau}{dt} - 3\frac{d\tau}{dt}$$

$$= 3k(1-\pi Z/3)^{\frac{1}{2}}(1-(1-\pi Z/3)^{\frac{1}{2}})$$

where $\frac{d\tau}{dt} = k = k_o \exp(-E/RT)$

Expressing k in terms of Z and $\frac{dZ}{dt}$, and then taking logarithm on both sides, we have

$$\ln\left\{\frac{1}{3}\left(\frac{1}{(1-\pi Z/3)^{\frac{1}{2}}}-1\right)\frac{dZ}{dt}\right\}=\ln k_o - E/RT \qquad (11)$$

Hence plotting the left hand side of (11) against 1/T should give a straight line graph with slope equal to -E/R and intercept ln k for $Z < .87$ (or $\tau < .16$). For $Z > .87$, differentiating equation (9) gives

$$\ln\left\{\frac{dZ}{dt}/(\pi^2(1-Z)\right\}=\ln k_o - E/RT \qquad (12)$$

For cubic particles of uniform sizes, similar development gives the following equations:

For $Z < .83$,

$$\ln\left\{\frac{dZ}{dt}(1-(1-Z)^{1/3})(1-Z)^{-2/3}(\tfrac{\pi}{6})\right\}=\ln k_o - E/RT \qquad (13)$$

For $Z > .83$,

$$\ln\left\{(4/3\pi^2)\frac{dZ}{dt}/(1-Z)\right\}=\ln k_o - E/RT \qquad (14)$$

Table 2.1 Equations For Fick's Law Solution

Particle Shape	$Z = (Q_t - Q_o)/(Q_\infty - Q_o)$	$Z' = \frac{dZ}{dt}$
Platelet	$Z = 1 - (8/\pi^2)\sum_{n=0}^{\infty}(2n+1)^{-2}\exp(-(2n+1)^2\,\pi^2\tau/4)$	$Z' = 2k\sum_{n=0}^{\infty}\exp(-(2n+1)^2\pi^2\tau/4)$
	$Z = 2(\tau/\pi)^{1/2}$ $(0 \le Z < 0.45)$	$Z' = k(\pi\tau)^{-1/2}$
	$Z = 1 - (8/\pi^2)\exp(-\pi^2\tau/4)$ $(.45 < Z < 1)$	$Z' = 2k\exp(-\pi^2\tau/4)$
Sphere	$Z = 1 - (6/\pi^2)\sum_{n=1}^{\infty} n^{-2}\exp(-n^2\pi^2\tau)$	$Z' = 6k\sum_{n=1}^{\infty}\exp(-n^2\pi^2\tau)$
	$Z = 6(\tau/\pi)^{1/2} - 3\tau$ $(0 \le Z < .87)$	$Z' = 3k((\pi\tau)^{-1/2} - 1)$
	$Z = 1 - (6/\pi^2)\exp(-\pi^2\tau)$ $(.87 < Z < 1)$	$Z' = 6k\exp(-\pi^2\tau)$
Cube	$Z = 1 - (512/\pi^6)\sum_{l=1}^{\infty}\sum_{m=1}^{\infty}\sum_{n=1}^{\infty}\frac{\exp(-\frac{\pi^2}{4}\tau(\sum_{j=1}^{n}(2j-1)^2))}{\prod_{j=1}^{n}(2j-1)^2}$	$Z' = (\frac{128k}{\pi^4})\sum_{l=1}^{\infty}\sum_{m=1}^{\infty}\sum_{n=1}^{\infty}\frac{\prod_{j=1}^{n}(2j-1)^2\exp(-\frac{\pi^2}{4}\tau\sum_{j=1}^{n}(2j-1)^2)}{\prod_{j=1}^{n}(2j-1)^2}$
	$Z = 1 - (1-2(\tau/\pi)^{1/2})^3$ $(0 \le Z < .83)$	$Z' = 3k(\pi\tau)^{-1/2}(1 - 2(\tau/\pi)^{1/2})^2$
	$Z = 1 - (\frac{512}{\pi^6})\exp(-3\pi^2\tau/4)$ $(.83 < Z < 1)$	$Z' = (\frac{384}{\pi^4})k\exp(-3\pi^2\tau/4)$

2.2 Desorption Controlled Kinetics

Consider an energetically uniform surface with all the active sites having identical activation energies of desorption, E. Assuming all the molecules are in the adsorbed state initially, the rate of desorption is proportional to the m-th power of the number of adsorbed molecules present, that is,

$$\frac{dn_a}{dt} = - k' n_a^m \qquad (15)$$

where n_a is the number of adsorbed molecules, m is the order of desorption, k' is the rate constant of desorption. The readsorption of desorbed molecules is assumed to be negligible for a sufficiently high flow of carrier gas. For first order kinetics, equation (15) may be written as

$$\frac{d(n_o-n)}{dt} = -k'(n_o-n)$$

or

$$\frac{dZ}{dt} = k'(1-Z) \qquad (16)$$

where n_o is the initial number of adsorbate molecules, n is the number of molecules in the gaseous state and Z is the fraction of molecules desorbed. The rate constant is assumed to be independent of surface coverage and its temperature dependence is given by the Arrhenius equation, $k' = k_o' \exp(-E/RT)$ The rate expression for a variable temperature process becomes

$$\frac{dZ}{dt} = k_o' \exp(-E/RT).(1-Z) \qquad (17)$$

Graphically a plot of ln $(\frac{dZ}{dt}/(1-Z)$ against 1/T should give a straight line if the first order kinetics holds.

For the second order kinetics,

$$\frac{dZ}{dt} = k'_o \exp(-E/RT).n_o^2 \ (1-Z)^2 \qquad (18)$$

Since n_o is a constant for a particular experiment, a plot of ln $(\frac{dZ}{dt}/(1-Z)^2)$ against 1/T should give a straight line with gradient equal to -E/R and intercept $k'_o n_o^2$. Table 2.2 gives a summary of the rate expressions and equations for integral data as well.

Table 2.2 Equations For Desorption Controlled Kinetics

Order of Desorption	$Z = (Q_t - Q_o)/(Q_\infty - Q_o)$	$Z' = \frac{dZ}{dt}$
1	$Z = 1 - \exp\left(-\int_0^t k' \exp(-E/RT)\, dt\right)$	$Z' = k' \exp(-E/RT).(1-Z)$
2	$Z = 1 - \left(1 + k'Q^2 \int_0^t \exp(-E/RT)dt\right)^{-1}$	$Z' = k'Q^2\exp(-E/RT).(1-Z)^2$
n	$\frac{((1-Z)^{1-n} - 1)}{1-n} = k'Q^n \int_0^t \exp(-E/RT)dt$	$Z' = k'Q^n\exp(-E/RT).(1-Z)^n$

2.3 Parabolic Law Solution

The Parabolic Law is based on the shell-progressive rate mechanism (24). The rate of reaction (the combustion of carbonaceous material within a porous catalyst, for example) depends only on the rate of the reactant gas diffusing into the particle. Gaseous reactant diffusing into the structure is assumed to be totally reacted with the reactant (usually solid phase dispersed in the particle) upon initial contact. Thus at any finite time after onset of the reaction, the surface of the remaining shell of solid reactant will react as fast as the gaseous reactant can diffuse to it through the porous structure.

In the present case of desorption of gas molecules having a diameter bigger than the pore openings of the solid, the structure of the solid may be damaged when the molecules are released at a high temperature. If it is postulated that this damage involves permanently enlarging the apertures, so that diffusivity in the damaged portion is large, the postulates of the Parabolic Law hold. Note that this is a reverse situation to the usual application of the Parabolic Law. If permanent damage occurs, subsequent adsorption on the solid should be changed.

Assuming uniform initial distribution and diffusion controlling, the desorption process may be described by the steady state diffusion equation with essentially no change in concentration with time in the region $R > r > r_b$ where

r_b is the boundary such that the concentration at r_b is the initial concentration C_o . The position of r_b at which the damage occurred moves radially inward. Noting that the fraction of gas desorbed, $Z = 1-(r_b/R)^3$, the solution of the diffusion equation

$$\frac{\partial^2(rC)}{\partial r^2} = 0 \qquad (19)$$

with boundary conditions $C=C_o$ at $r = r_b$ and $C = 0$ at $r = R$, can be shown to be

$$\frac{1-Z}{3} - \frac{(1-Z)^{2/3}}{2} + 1/6 = \tau \qquad (20)$$

where $\tau = \int_o^t D/R^2 \, dt$. The rate expression may be obtained by differentiating equation (20) to give

$$\frac{dZ}{dt} = 3(D/R^2)((1-Z)^{-1/3} - 1)^{-1} \qquad (21)$$

Table 2.3 gives the equations for other geometries.

Table 2.3 Equations For Parabolic Law Solution

Particle Shape	$Z = (Q_t - Q_\circ)/(Q_\infty - Q_\circ)$	$Z' = \frac{dZ}{dt}$
Platelet	$Z = (2\tau)^{\frac{1}{2}}$	$Z' = k''/Z$
Sphere	$\frac{1-Z}{3} - \frac{(1-Z)^{2/3}}{2} + 1/6 = \tau$	$Z' = \frac{3k''(1-Z)^{1/3}}{(1-(1-Z)^{1/3}}$
Cube	$Z = 1 - (1 - (2\tau)^{\frac{1}{2}})^3$	$Z' = \frac{3k''(1-Z)^{2/3}}{(1-(1-Z)^{1/3}}$

2.4 Theoretical Model to Simulate the TPD Spectra

Consider cubic crystals, as observed (22) for Type A zeolites, the exact solution for Fick's Second Law of diffusion (21) is

$$1 - Z = \frac{512}{\pi^6} \sum_{l=1}^{\infty} \sum_{m=1}^{\infty} \sum_{n=1}^{\infty} \exp\left\{ \frac{\pi^2 \tau \left((2l-1)^2 + (2m-1)^2 + (2n-1)^2 \right)}{(2l-1)^2 (2m-1)^2 (2n-1)^2} \right\} \tag{24}$$

The equation can be simplified using the relation

$$1 - Z_{cube} = \left(1 - Z_{platelet} \right)^3 \tag{25}$$

and this will be discussed subsequently. Now, let the rate of desorption be $\frac{dZ}{dt} = F(\tau, x)$, where x is the half side length of a cube. To take into consideration the effect of particle size distribution, the average rate of desorption becomes

$$\overline{\frac{dZ}{dt}} = \int_{-\infty}^{\infty} p_x(x) \, \frac{dZ}{dt}(\tau, x) \, dx \tag{26}$$

where $p_x(x)$ is the probability distribution function in terms of weight of the particle sizes. For small particles (26), $p_x(x)$ would be a log-normal distribution function.

$$p_x(x) = \frac{1}{(2\pi)^{\frac{1}{2}} x \ln \sigma} \exp\left(- \left(\frac{\ln(x/\mu)}{2^{\frac{1}{2}} \ln \sigma} \right)^2 \right) \tag{27}$$

where μ is the weight average particle size,

$$\sigma = \frac{\text{size below which 50 wt \% of particles lie}}{\text{size below which 15.87 wt \% of particles lie}}$$

and $p_x(x)dx$ is the weight fraction of particles with sizes between x and x + dx.

Usually the probabilty distribution function $p_x(x)$ determined from the log-normal probability plot is in terms of the entire length of the particle. Thus, a transformation $y = x/2$ is used to obtain the proper probability distribution function $p_y(y)$. It is shown (27) that

$$p_y(y) = 2\, p_x(\, 2y\,)$$

$$= \frac{1}{(2\pi)^{\frac{1}{2}} y \ln \sigma} \exp\left(- \left(\frac{\ln(y/\mu')}{2^{\frac{1}{2}} \ln \sigma} \right)^2 \right) \qquad (28)$$

where $\mu' = \mu / 2$

Putting $w = \ln(y/\mu') / (2^{\frac{1}{2}} \ln \sigma)$ and $dw = (d\ln y) / (2^{\frac{1}{2}} \ln \sigma)$

equation (26) becomes

$$\frac{dZ}{dt} = \frac{1}{\pi^{\frac{1}{2}}} \int_{-\infty}^{\infty} \exp(- w^2) \frac{dZ}{dt}(\tau, w)\, dw \qquad (29)$$

The integration may be simplified by noting that

$$\int_{-\infty}^{\infty} \exp(- w^2)\, f(w)\, dw = \sum_{i=1}^{m} H_i\, f(w_i)$$

where m is the order of the Hermite polynomial $H_m(w)$, w_i's are the roots of $H_m(w) = 0$ and H_i are the weighting factors (Appendix C-1).

CHAPTER 3

EXPERIMENTAL

3.1 Pretreatment of the Sample

About 2 g of the powder material (Linde 3A Zeolite Molecular Sieve) were evacuated in a sample tube (Fig. 3.1) 450°C and a pressure of less than 10^{-5} torr for 15 hours using a mercury diffusion pump backed by a conventional rotary oil pump. Most of the water that was present in the original sample should be removed at 400°C. The weight loss upon evacuation was 17 % to 19 %. Desorption data were calculated per gram of the dry sample.

3.2 Encapsulation

The sample was heated under pressure to introduce gas at high temperature and pressure and then cooled to room temperature. The sample tube was transferred to the autoclave (Fig. 3.2) in a stream of dry adsorbate gas so that no moisture may be in contact with the sample when the sample tube was uncapped. The system was evacuated by a rotary vacuum pump to remove any air present before charging the autoclave to the maximum pressure of a gas cylinder. For size 1A prepurified nitrogen or argon the pressure at full capacity is about 2200 psia. The bolts fastening the head to the autoclave were tightened in an orderly manner using a torque wrench with a torque of 80 lb.ft. A leak test was performed

with soap solution at pressure and room temperature. Any leakage was due to dirt or worn-out gaskets. The pressurised system was then heated to 350°C and held at that temperature. The pressure was noted on the pressure gauge and the temperature, controlled manually by a variable transformer, was recorded on a recorder chart. After 8 hours of heating, the autoclave was cooled to room temperature. The pressure at room temperature was noted. After the pressure was released, a stream of dry adsorbate gas was passed through the autoclave and the head was then removed. The sample tube was greased and capped before removing it from the autoclave.

3.3 Temperature Programmed Desorption (TPD)

The sample was transferred to the TPD tube (Fig.3.3) inside a dry box (Fig. 3.4) in which dry nitrogen was maintained at a pressure slightly higher than atmospheric. The dry box was flushed with dry nitrogen thrice by means of a pump in order to remove any moisture present. Before desorption the sample in the desorption tube was evacuated at room temperature for half of an hour.

Thermal desorption was carried out in a dynamic system using helium as a carrier gas. The temperature of the electrical furnace, used to heat the sample, was linearly increased by driving at a constant rate the potentiometer knob of a proportional controller. The chromel-alumel thermocouple located in the sample was used to measure the temperature

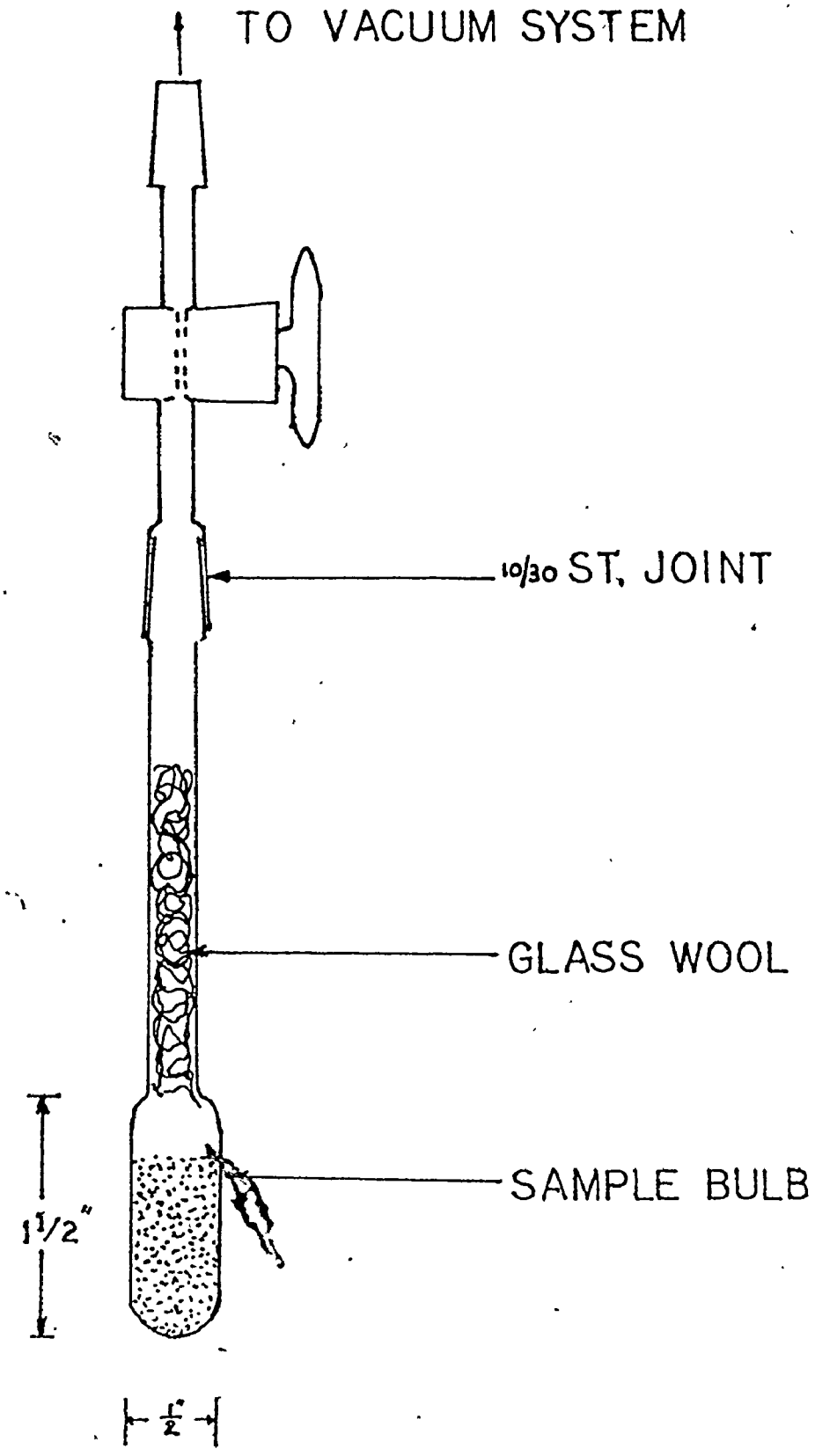

FIG 3.1 SAMPLE TUBE

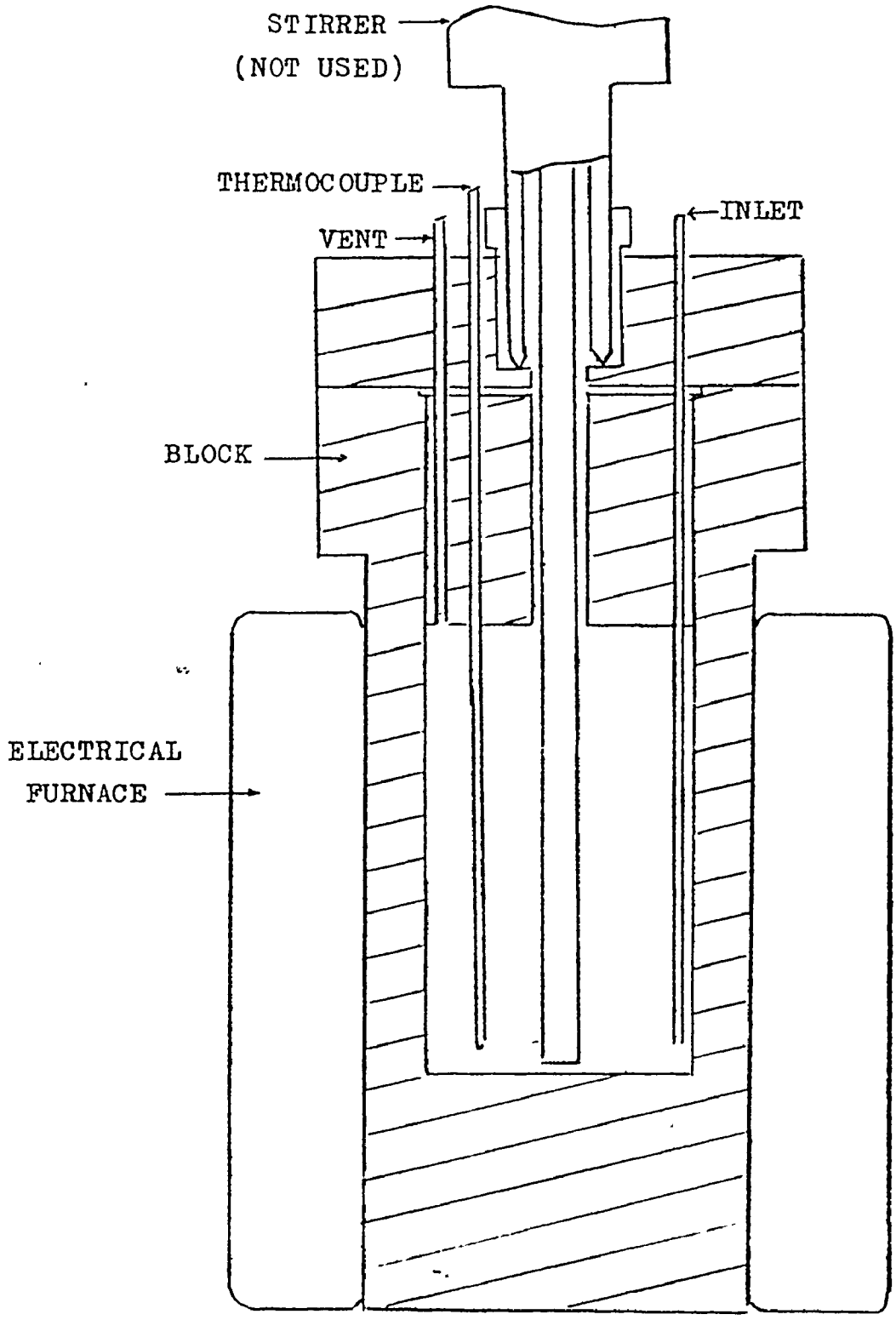

Figure 3.2 The Autoclave

FIG 3.3 TPD DESORPTION CELL

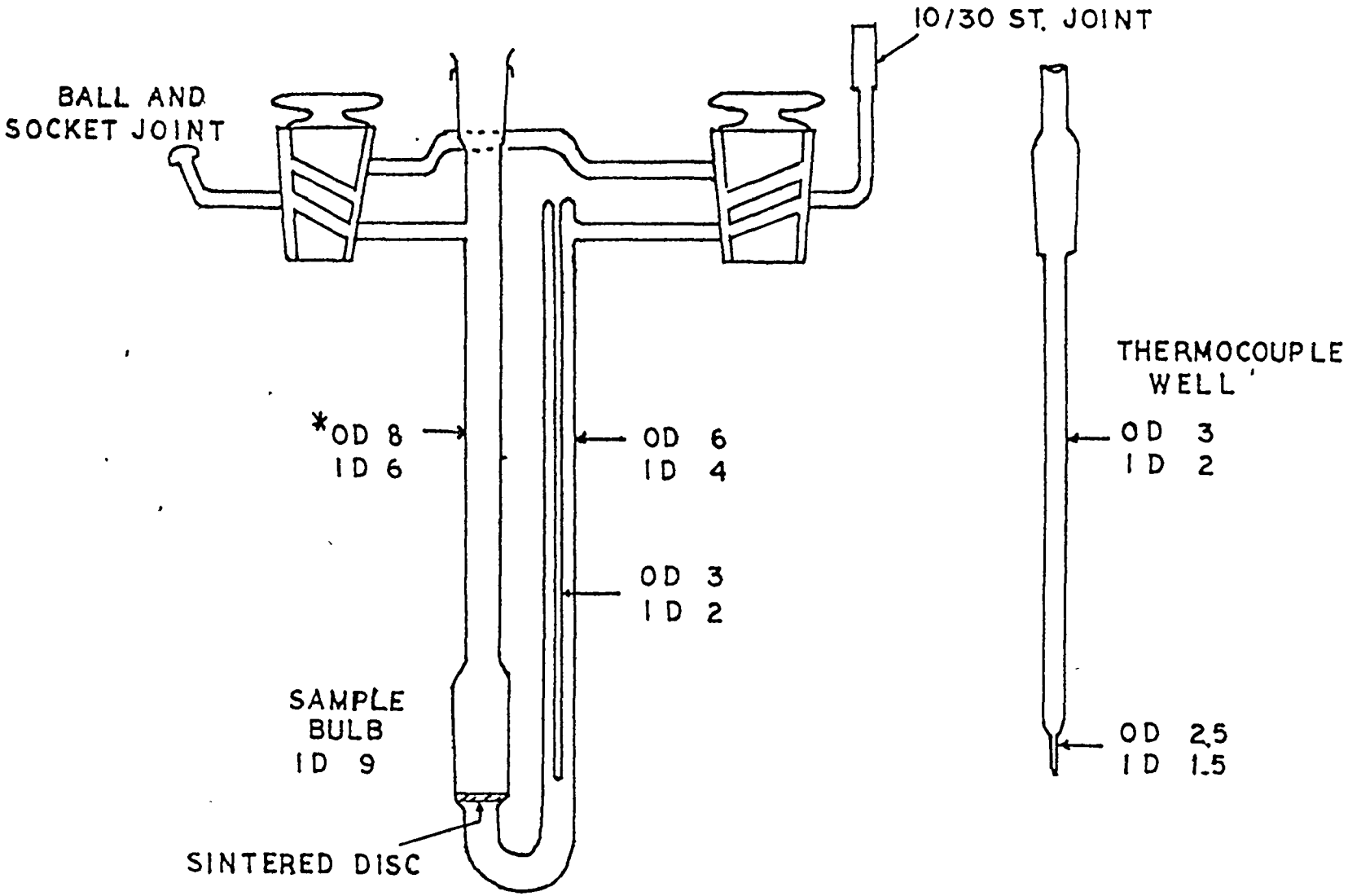

* The dimensions are in millimeters

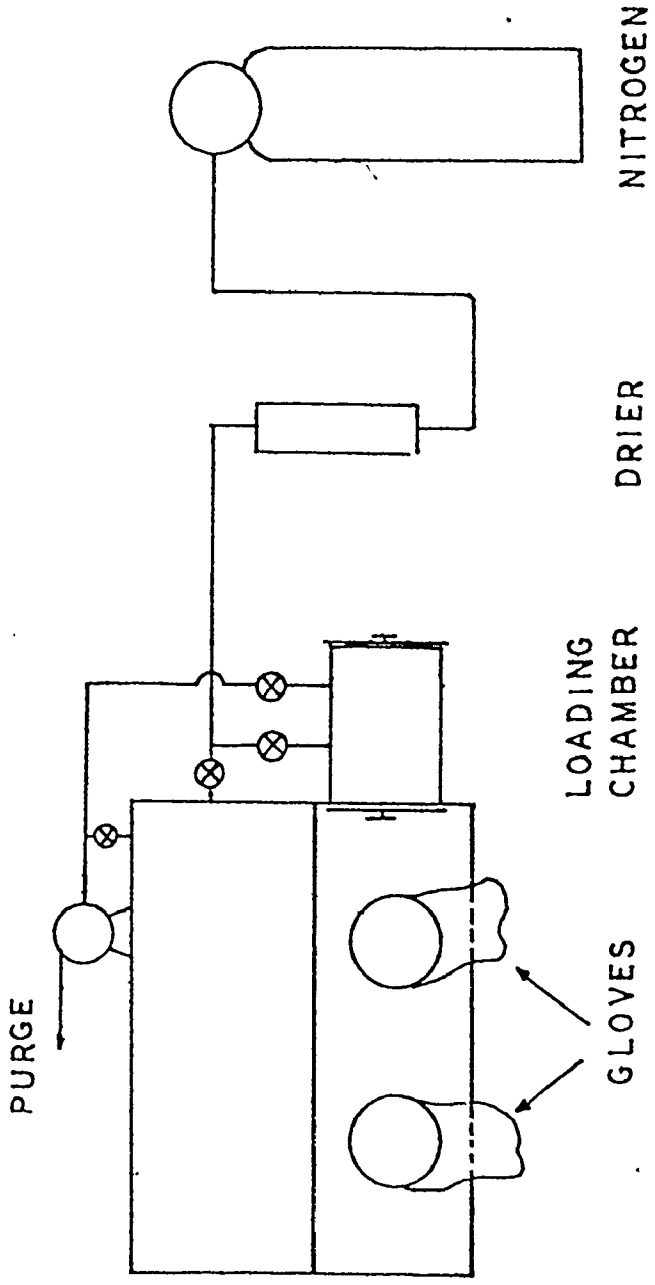

FIG 3.4 DRY BOX

of the powder using a digital voltmeter. By changing the size of the rubber wheel attached to the shaft of a synchronous motor or changing to another motor with a different speed, the heating rate can be varied accordingly. The range of heating rate used in the present work was from 3°C/min. to 17°C/min. A carrier gas flowrate of 40 ml/min was used. Too low a flowrate gave unsteady responses whereas too high a flowrate gave a small response. No flowrate changes were observed at room temperature and a steady base line on the recorder chart was maintained for at least three hours before each experiment was started. However, the flowrate decreased as temperature of the sample increased, e.g. by 2 ml/min at 500°C, owing to the increase of viscosity of gas through the sample in the desorption tube. The heating rate was fairly constant as shown in Fig. 3.5 ; the rate decreased a little at high temperatures above 500°C since the rate of heat lost to the environment is high at high temperature. The heating rate was linear in the region where desorption occurred.

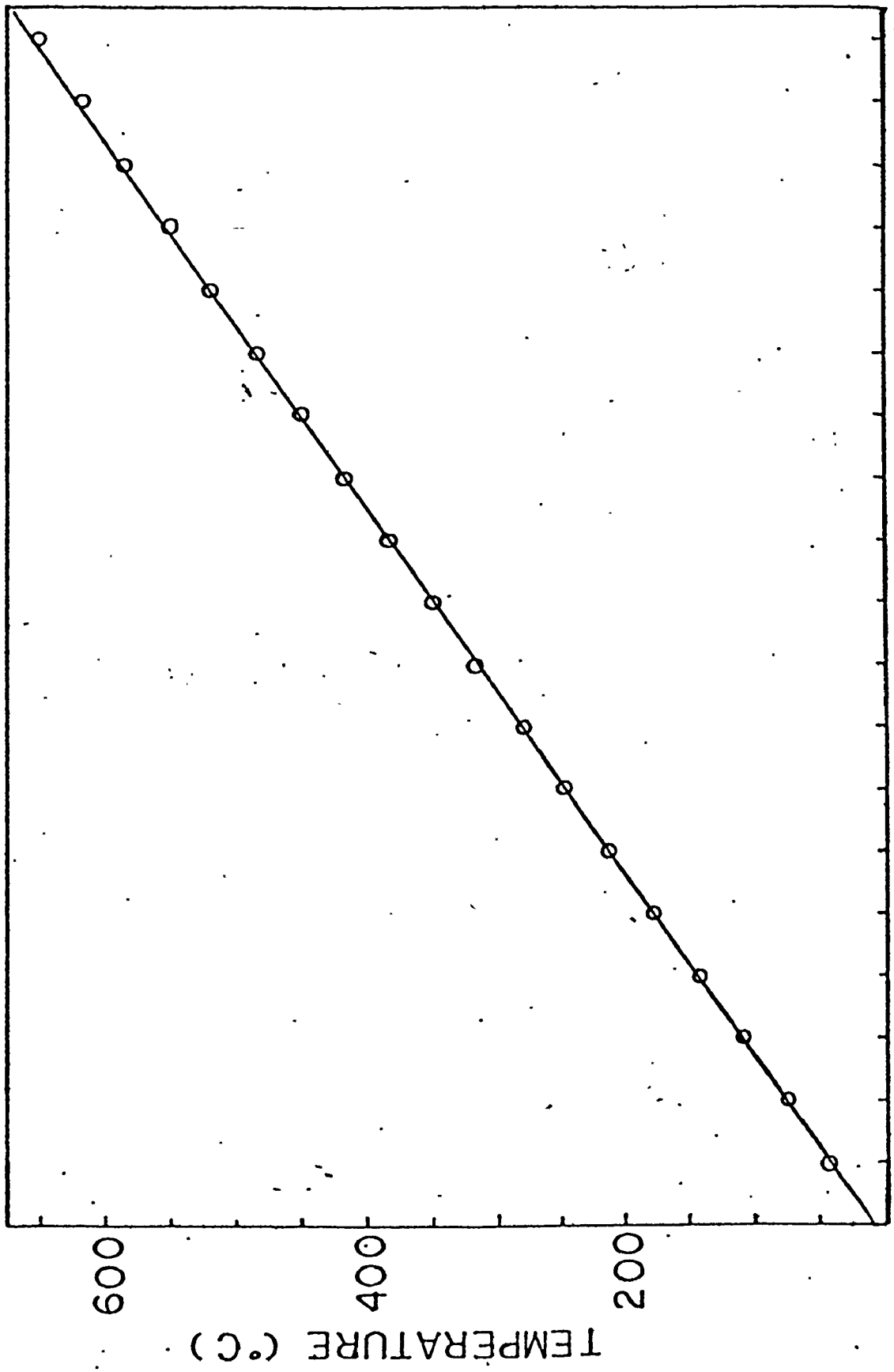

FIG. 3.5 TEMPERATURE VS. TIME

3.4 The Flow System

A flow diagram of the apparatus is shown in Fig.3.6. The carrier gas, helium, at 15 psig. from the regulator, passed through a needle valve, flowmeter, cold trap, reference side of the thermal conductivity cell (TCC), desorption tube, cold trap and then the detection side of the TCC. The TCC (Gow-Mac Model 10-952) with tungsten filaments was used to detect the concentration of desorbed gas. The flowrate was read on the flowmeter which was calibrated with a soap-film flowmeter. The advantage of the flowmeter is that readings can be taken without disturbing the flow of the system. Two dry ice - acetone cold traps (at -78°C) were used to trap any water vapour present in the carrier gas or in the desorbed gas stream. A water vapour saturation tube was also incorporated so that water vapour could be introduced into the carrier gas stream if desired. The saturation tube was operated at room temperature, the saturation vapour pressure being 23.7 torr at 25°C. An injection valve was used to calibrate the response of the recorder using different loops of known volume. One of the disadvantages of using fine powder in the desorption tube is that the viscosity of gas increases with temperature resulting in a decrease of flowrate of 2 ml/min between room temperature and 500°C. The lower flow caused a small change in concentration (about 5 %) but the base line remained constant.

An A/C voltage stabilizer (Model SF-3-L-R, Watford Control Instrument Ltd.) was used to regulate the line voltage of the system. The signal response was recorded on a

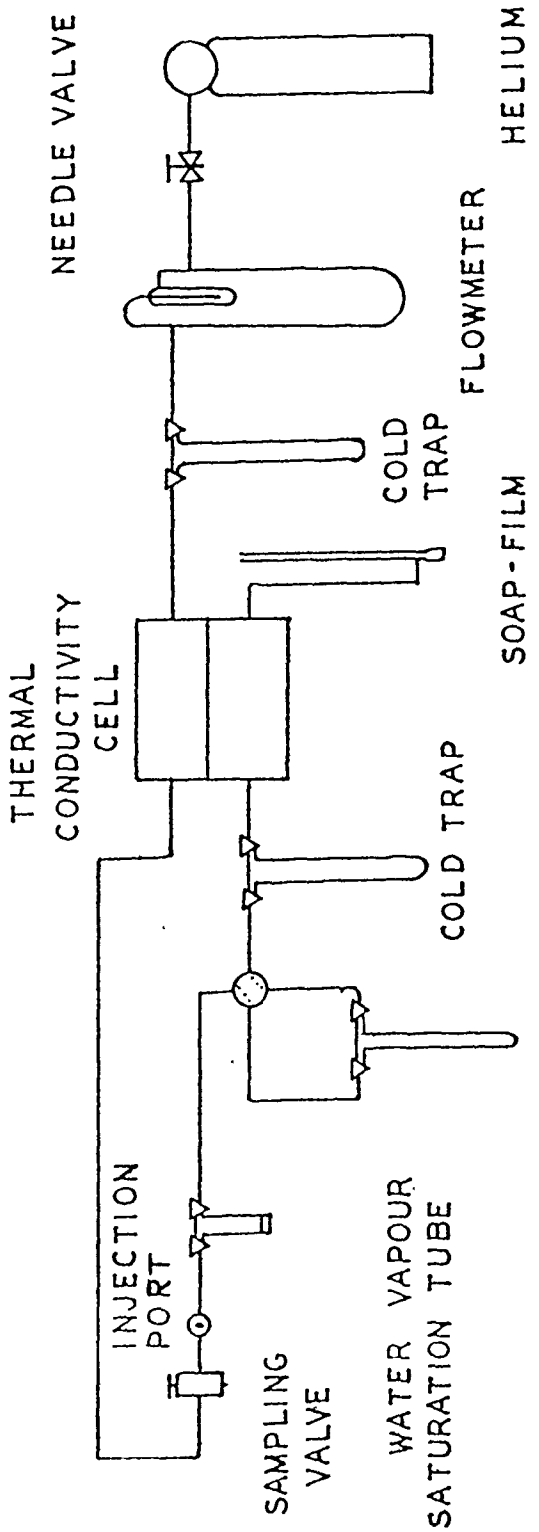

FIG. 3.6 EQUIPMENT FLOWSHEET

recorder (Texas Instruments Servoriter II) with a Ball and Disc integrator.

The U-shaped desorption tube (Fig. 3.3) was made of quartz so that temperature up to 1000°C might be used. Graded-seals were used to attach quartz to Pyrex in the portion of the tube that was subjected to temperature lower than 550°C. A quartz sintered disc was used to support the powder sample. Two thermocouples were used: One located in the sample was connected to the digital voltmeter to measure the temperature of the sample, and the second one located in the other arm of the TPD tube was connected to the controller. The time lag from the desorption tube to the detector was about 22 seconds for a flow of carrier gas of 40 ml/min. This factor was taken into account in the analysis of data.

3.5 Volumetric Apparatus

A volumetric apparatus equipped with a manostat and a calibrated burette was also used to measure the absolute amount of gas evolved from the sieve by thermal desorption. Fig. 3.8 shows a schematic diagram of this constant pressure, variable volume system. The system consists of five bulbs of calibrated volumes (25) of 4.60, 16.31, 22.76, 49.42, and 135.06 c.c.; a calibrated graduated burette of 100 c.c. capacity and a mercury manometer, all connected by capillary tubing to the sample tube and to a vacuum system and gas storage system.

The pressure in the system could be maintained constant by the lowering or raising of a mercury levelling bulb which was connected to the calibrated burette by rubber tubing. A sealed trap which is not shown, was used to trap any air which might diffuse through the tubing. During desorption experiments the levelling bulb was automatically lowered in small steps by a motor which was turned on when mercury in the left leg of the manometer was out of contact of an electrode at the zero reference mark. Similarly for adsorption the levelling bulb was raised automatically by the motor when mercury touched the electrical contact.

The temperature of the gas bulbs and burette was maintained at 30°C, the temperature at which their volumes had been calibrated, by circulating water through jackets from a constant temperature bath. The temperature of the sample was measured by a chromel-alumel thermocouple.

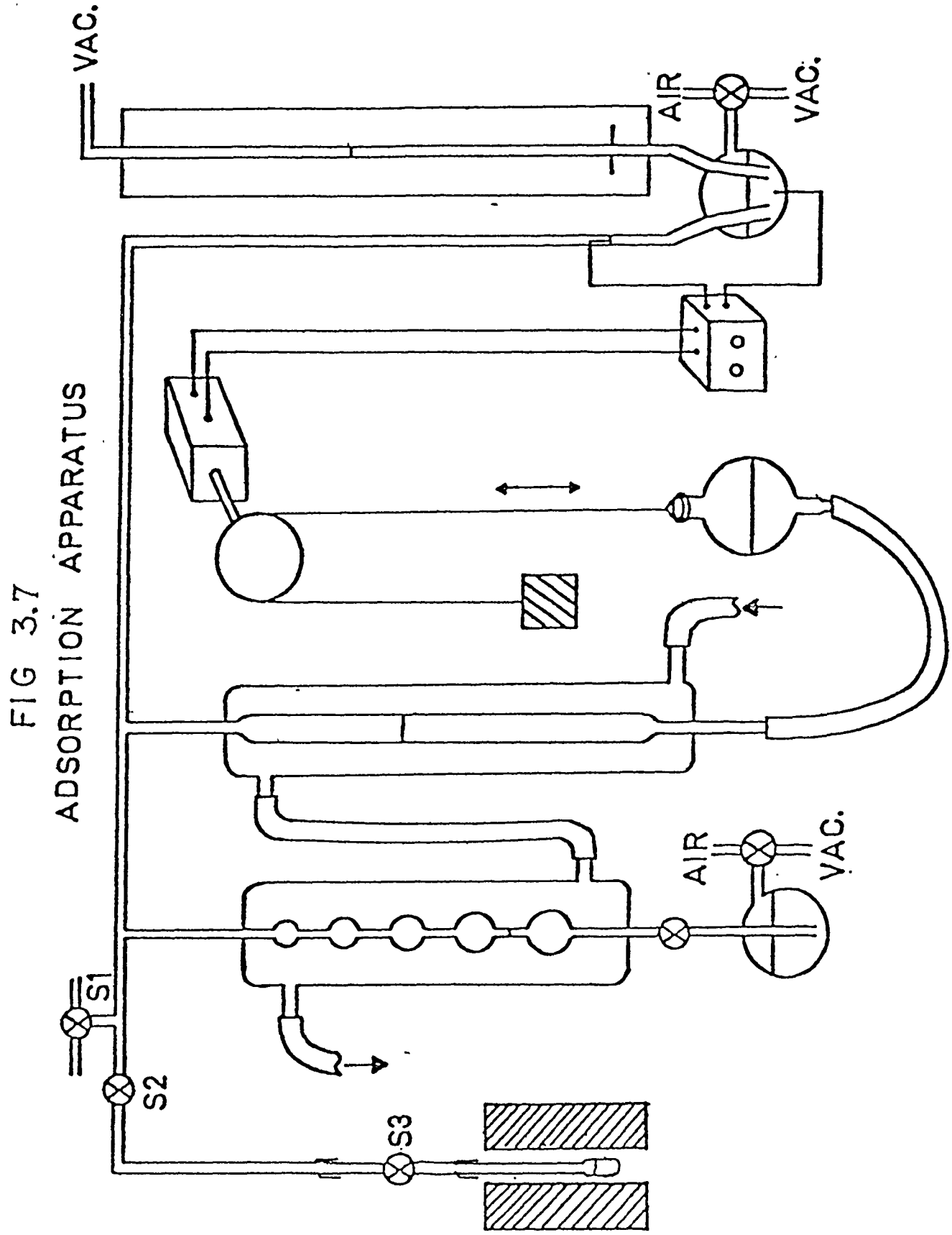

FIG 3.7
ADSORPTION APPARATUS

The void space (V_v), the volume of the capillary tubing to the right of S2 in Fig.3.8 was determined as 11.79 c.c. at room temperature by the method given in Appendix A-1.1 . Dead space factor was determined by helium which is not supposed to be adsorbed by the molecular sieve. The dead space volume, the volume of gas in c.c.(S.T.P.) per unit pressure in the sample tube and the space below S2, not including the amount of gas adsorbed on the sample, was measured at several temperatures between -78°C to 500°C., following the method given in Appendix A-1.2 . Before desorption the entire system was evacuated via S1 until a good vacuum (less than 10^{-5}torr) as indicated by a McLeod gauge (not shown) was obtained. The total amount desorbed at a temperature up to 550°C was measured when no further change in volume was observed in 2 hours. The amount of gas desorbed was $Q_\infty = (V_v + V_{bulbs} + V_{burette} + V_{dead\ space})/W$ c.c.(S.T.P.) per gram of dry zeolite (W = sample weight (g)).

3.6 Particle Size Measurement

About 2 g of the molecular sieve powder were dispersed in 100 ml of methanol. An aqueous ammonia solution was tried but the particles were not dispersed very well. Methanol seemed to separate the crystal aggregates better. Probably the rapid evaporation facilitates the dispersion of particles on the film. A tiny drop of standard latex material of very narrow size range (diameters of 0.234 microns ± 4 %) was added to the suspension. A thin film of formwar on top of a copper grid (200 mesh) was placed on a microscopic slide. The suspension of the powder, after being stirred vigorously for half of an hour, was sprayed onto the formwar film. In order to improve electrical conductivity a thin film of carbon was coated onto the grids prior to insertion into the microscope.

Micrographs were taken using a Phillips Transmission Electronmicroscope at various magnifications ranging from 4500X to 1300 X. The microscope was operated at a voltage of 100 kV. About 400 particles were counted. The particles were cubic in shape, but larger ones (sizes larger than 2 microns) apparently have their corners 'chopped off' at 45° to the main faces. Fig. 3.11 shows two typical micrographs.

The histogram in Fig. 3.8 describes the weight distribution of particle sizes. Normal probability distribution (Fig.3.9) fits the data fairly well but this may involve negative particle sizes in some calculations. The log-normal probability distribution (Fig. 3.10) avoids this problem of negative particle

Table 3.1 Particle Size Distribution Data

Edge Length (Microns)	Frequency	Wt Fraction	Cumulative Wt Fraction
0.2	5	.0000	.000
0.4	11	.0000	.000
0.6	25	.0007	.001
0.8	20	.0013	.002
1.0	22	.0028	.005
1.2	20	.0045	.009
1.4	25	.0089	.018
1.6	24	.0127	.031
1.8	33	.0249	.056
2.0	26	.0269	.083
2.2	32	.0440	.127
2.4	18	.0320	.159
2.6	15	.0340	.193
2.8	22	.0624	.255
3.0	13	.0454	.300
3.2	11	.0466	.347
3.4	19	.0965	.444
3.6	7	.0422	.486
3.8	9	.0638	.550
4.0	12	.0992	.649
4.2	9	.0862	.735
4.4	2	.0220	.757
4.6	3	.0377	.795
4.8	3	.0429	.838
5.0	0	.0000	.838
5.2	1	.0182	.856
5.4	0	.0000	.856
5.6	0	.0000	.856
5.8	1	.0252	.881
6.0	0	.0000	.881
6.2	0	.0000	.881
6.4	1	.0339	.915
6.6	0	.0000	.915
6.8	1	.0406	.955
7.0	1	.0443	1.000

FIG 3.8 PARTICLE SIZE DISTRIBUTION

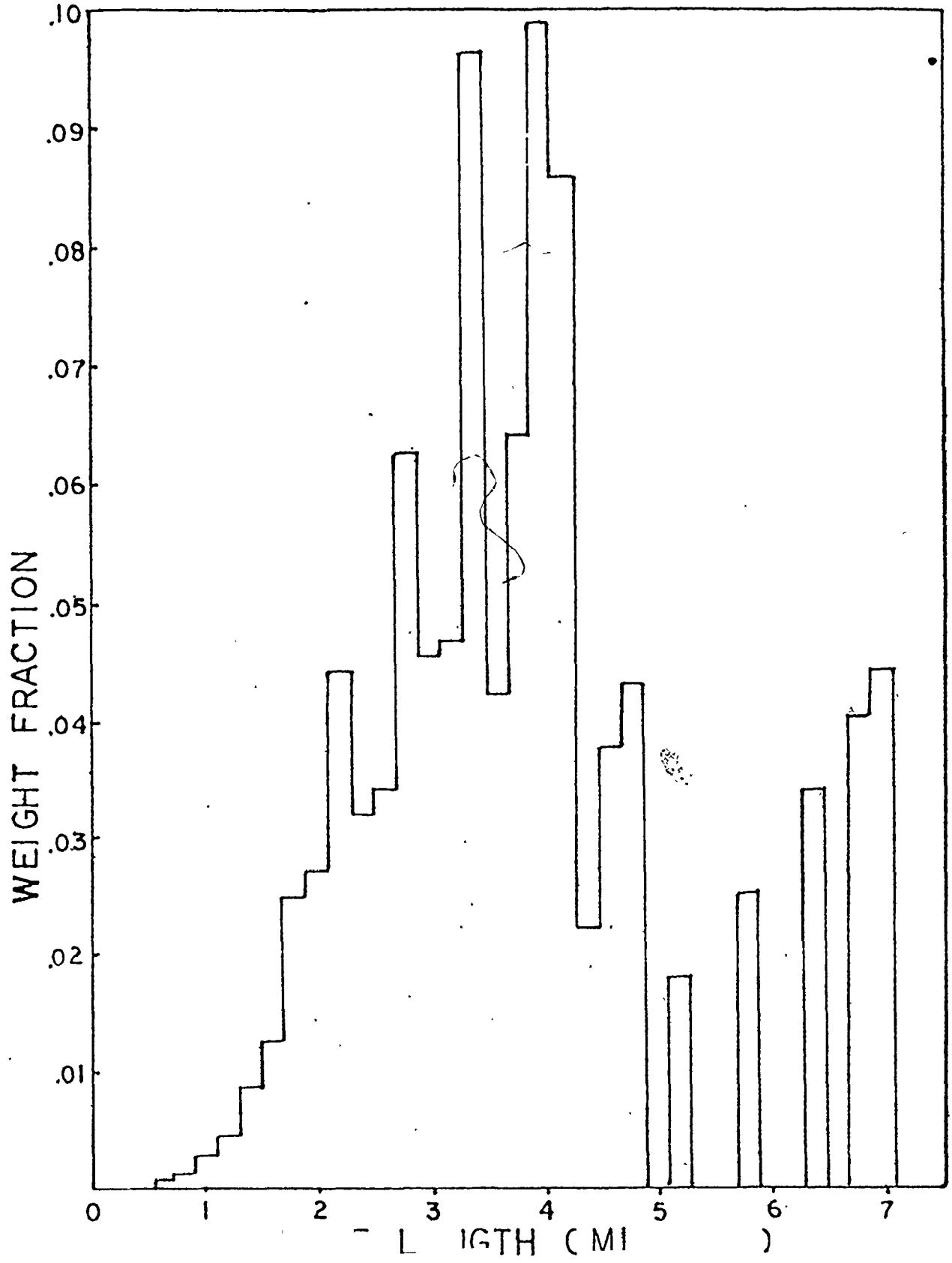

FIG.39 NORMAL DISTRIBUTION OF PARTICLE SIZES

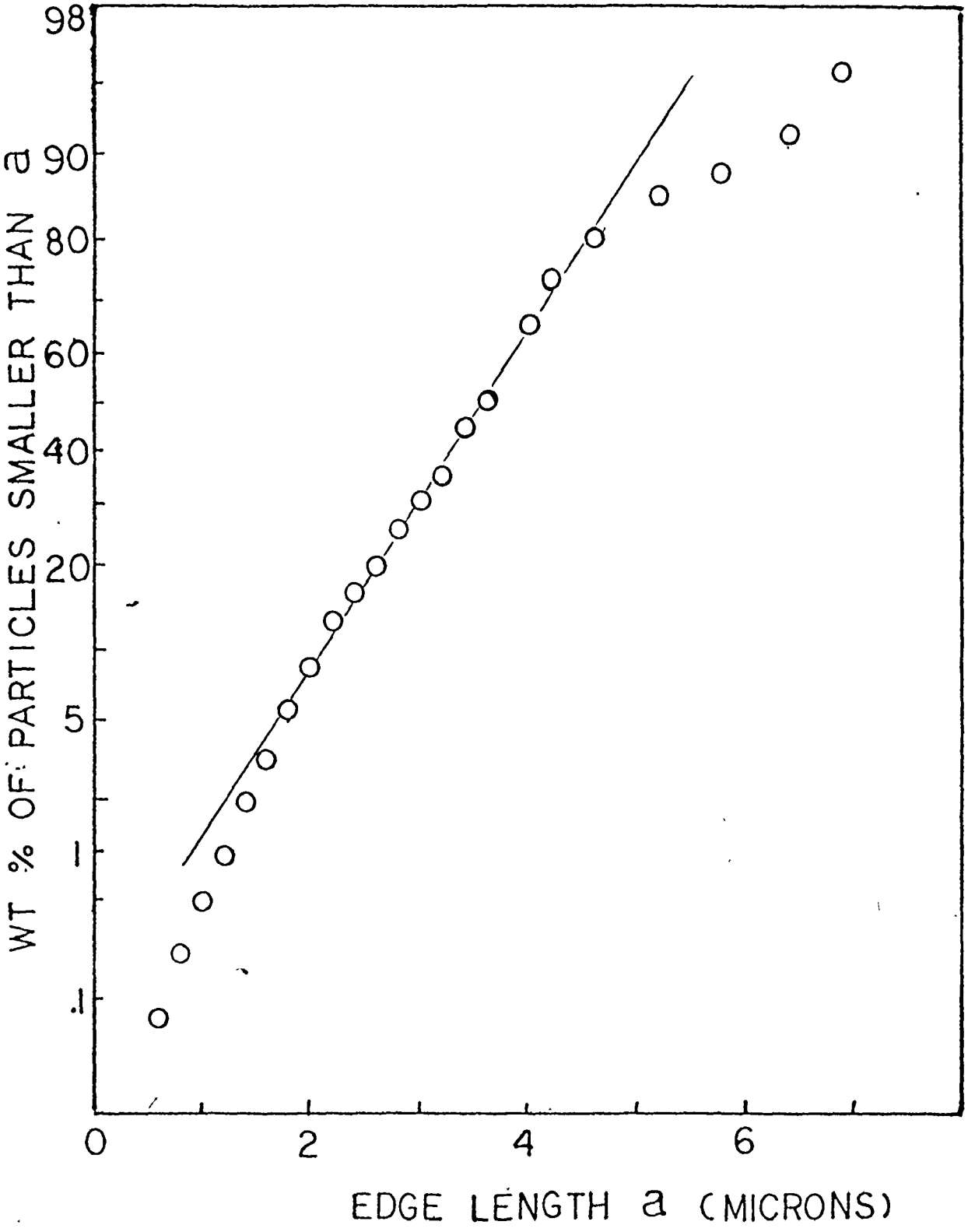

FIG.3.10 LOG-NORMAL DISTRIBUTION OF PARTICLE SIZES (WT. BASIS)

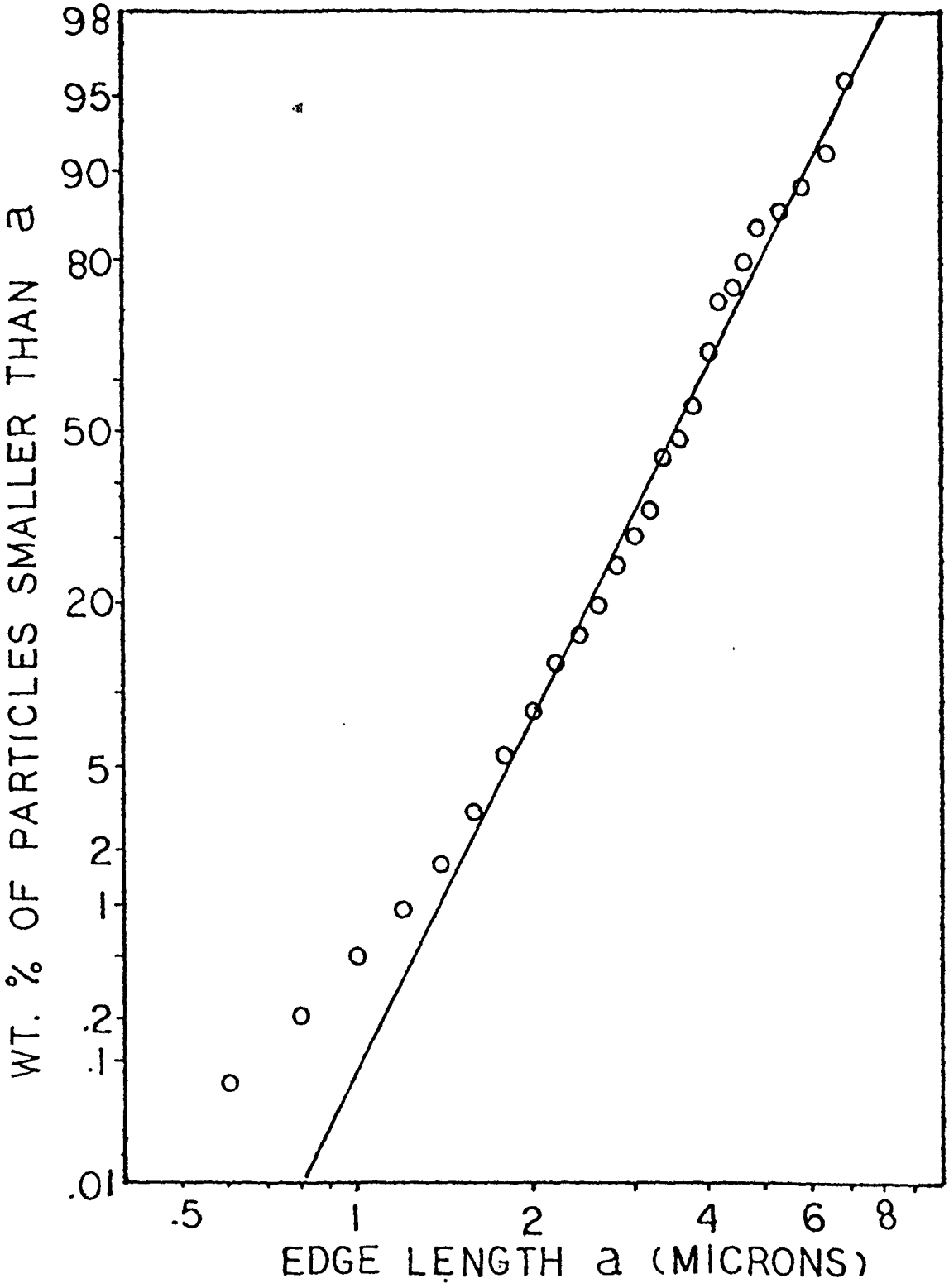

Figure 3.11

Micrographs of 3A Crystals

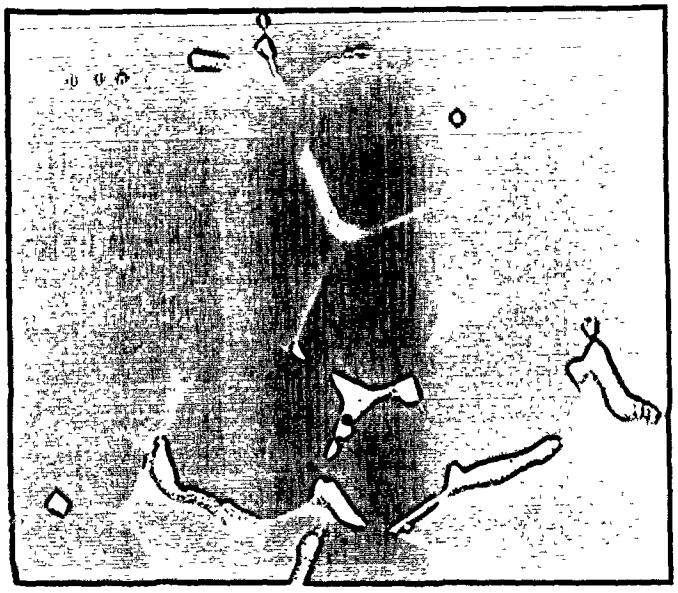

4600 X

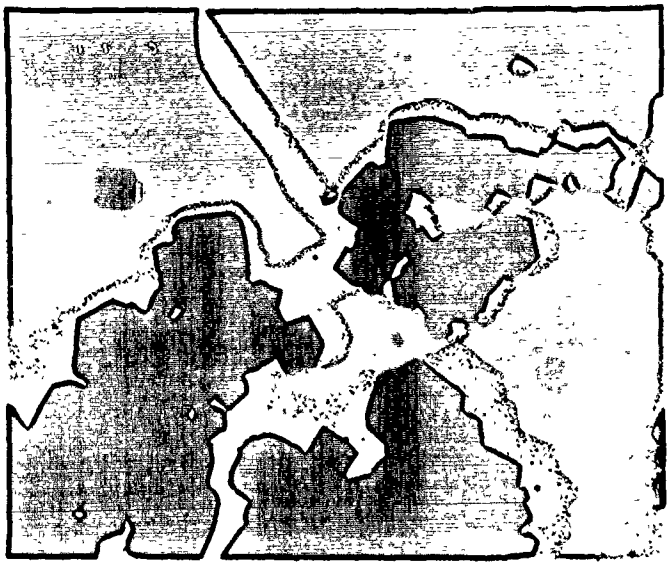

3000 X

sizes and seems to fit the data well for particle sizes larger 1 micron. The weight average size was found to be 3.5 microns and the standard deviation was 1.49 microns. The values indicate that the 3A particles are smaller and more broadly distributed than 4A particles as measured by Eagan (22) with a weight average of 4 microns and standard deviation of 1.33 microns.

3.7 Chemical Analysis

In Type A zeolites the ratio of Si/Al is 1. Potassium ion is introduced in 3A by potassium ion exchange. Here we wish to find out the relative amount of the potassium and sodium ions present in the sample. About 1 g of molecular sieve powder was dissolved in 1 N solution of hydrochloric acid. The solution was analysed by Mr. M.Van Oosten using Atomic Absorption Spectrophotometry (28). The principle of atomic absorption is based on dissociation of the element of interest into its ground state by heating the sample in a flame. The element is then capable of absorbing radiation at discrete lines of narrow bandwidth called ground state, or resonance, lines. The narrow emission lines are provided by a hollow-cathode lamp which contains a cathode made of the element being sought and is filled with neon or argon at a low pressure. The resonance line for sodium is 5896 Å and potassium is 7665 Å. Hydrogen-air flame was used for both determinations. The results of analysis are shown in Table 3.2.

Table 3.2

Result of Atomic Absorption Spectrophotometry Analysis

Sample Number	Result of Analysis	Average (g)
Nal	.0471; .0475	.0473
Kl	.078 ; .079	.0785

The ratio of the number of atoms of Na and K is

$$\frac{Na}{K} = \frac{(.0473)/23}{(.0785)/39.1} = 1.02$$

Thus, the present sample is about 50 % potassium exchanged NaA.

3.8 X-ray Spectra

To find if there was any change of the crystal structure in the thermal desorption, X-ray powder diffraction patterns were obtained for the samples desorbed at 400°C and 700°C. A Debye-Scherrer camera (29) was used. The wavelength of the X-rays is that for Copper K radiation, 1.5418 Å. The sample was put into a fine glass capillary of about 0.1 mm diameter. All the samples used were hydrated. The exposure time for each of these was 4 hours. The spectra obtained were compared with the fresh molecular sieve powder. A film reader with a vernier scale was used to interpret the lines.

The results (Table 3.3) show that the lattice parameter remains the same (12.30 Å) for all samples. The peak intensities of the desorbed samples seemed to be weaker than those of the fresh sample. Most of the lines were identified with those for the fresh sample indicating that the d-spacings in the crystal did not change.

The factors affecting the intensity of the powder diffraction pattern include the amount of sample used, the diameter of the capillary, degree of hydration, temperature as well as the time of exposure. Since all the samples were treated under the same conditions, with the same current and exposure time, it is possible that the loss in intensity is due to disruption of silica-alumina network. However, adsorption of nitrogen at -78°C on samples

desorbed at 400°C showed that none of these samples adsorbed appreciable amounts of nitrogen. Only 3 c.c.(S.T.P.)/g were adsorbed as compared to 60 c.c.(S.T.P.)/g for 4A zeolites which have pore openings of 4 Å in diameter. Hence, it is concluded that nitrogen did not penetrate and adsorb in the cavities of 3A molecular sieves.

Table 3.4 compares the X-ray powder diffraction patterns of present samples with those given in the literature (30,31). Both sodium and potassium ions were shown to be present in the sample and the intensities are different for different degree of potassium ion exchange.

Table 3.3 X-ray Diffraction Patterns of Desorbed Samples

Fresh Sample			Sample Desorbed at 400°C			Sample Desorbed at 700°C		
θ	d	I	θ	d	I	θ	d	I
7.2	12.30	S	7.2	12.30	S	7.2	12.30	S
10.2	8.71	S	10.0	8.87	S	10.0	8.88	S
12.5	7.12	M	11.2	7.94	M	12.4	7.18	W
16.2	5:53	M	15.9	5.63	W	15.9	5.63	VW
17.5	5.13	VW	-	-	-	-	-	-
20.4	4.42	VW	-	-	-	-	-	-
21.7	4.17	S	21.6	4.19	M	21.6	4.19	M
22.8	3.98	W	-	-	-	22.9	3.96	W
24.0	3.79	S	23.9	3.81	S	23.8	3.82	S
25.0	3.65	VW	-	-	-	-	-	-
26.0	3.52	M	26.0	3.52	W	26.0	3.52	W
27.2	3.37	S	27.1	3.38	M	27.1	3.38	M
29.0	3.18	W	29.1	3.17	W	-	-	-
29.9	3.09	S	29.9	3.09	S	29.8	3.10	S
30.9	3.00	M	30.7	3.02	W	-	-	-
32.6	2.86	M	32.4	2.88	M	32.5	2.87	W

Intensity: S - Strong; M - Medium; W - Weak; VW - Very Weak

Table 3.4 X-ray Diffraction Patterns of the Present Fresh Sample Compared with Literature Data

	$Na_{12}A$ (30,31)		$K_{12}A$ (30,31)			Present Fresh Sample	
hkl	d (Å)	I	d (Å)	I	θ	d (Å)	I
100	12.29	100	12.31	100	7.2	12.30	S
110	8.71	69	8.71	64	10.2	8.71	S
111	7.11	35	7.10	30	12.5	7.12	M
200	-	-	6.15	4	-	-	-
210	5.51	25	5.50	10	16.2	5.53	M
211	5.03	2	5.03	8	17.5	5.13	VW
220	4.36	6	-	-	20.4	4.42	VW
221,300	4.107	36	4.105	33	21.7	4.17	S
310	-	-	3.895	10	22.8	3.98	W
311	3.714	53	3.714	62	24.0	3.79	S
222	-	-	3.555	5	25.0	3.65	VW
-	-	-	-	-	26.0	3.52	M
320	3.417	16	3.414	34	27.2	3.37	S
321	3.293	47	3.292	35	29.0	3.18	W
400	-	-	3.098	12	29.9	3.09	S
410	2.987	55	2.985	80	30.9	3.00	M

Intensity: S - Strong; M - Medium; W - Weak; VW - Very Weak

CHAPTER 4

EXPERIMENTAL RESULTS AND DISCUSSIONS

Rate data were determined on 3A zeolite for nitrogen, argon and carbon dioxide. A typical plot of the TPD spectra for the three gases, at a particular heating rate (about 17°C/min.), is shown in Fig. 4.1. The rate $\frac{dZ}{dt}$ is plotted against time. The spectra for N_2 and CO_2 have only one peak whereas the spectrum for Ar has two peaks, one occurring at 350°C, and the other at about 500°C. The result will be discussed subsequently.

4.1 Encapsulation

The amount of gas trapped in the molecular sieve was determined by measuring the volume of gas evolved by thermal desorption. The data for various encapsulations of Ar, N_2 and CO_2 were given in Table 4.1. The amount measured in the TPD apparatus agrees within ± 1 c.c./g compared with that measured in the volumetric apparatus. The sizable amount of gas per gram trapped in 3A indicates that at high temperature the diffusivity increases tremendously such that gases not being adsorbed at normal adsorption conditions can penetrate the apertures of the sieves whose sizes are smaller than those of the incoming gas molecules.

Ar and N_2 have comparable amounts trapped under almost the same temperature and pressure (350°C and 1800 psig.), but much less than the amount of CO_2 trapped at a lower pressure (800 psig.). If the adsorption capacity

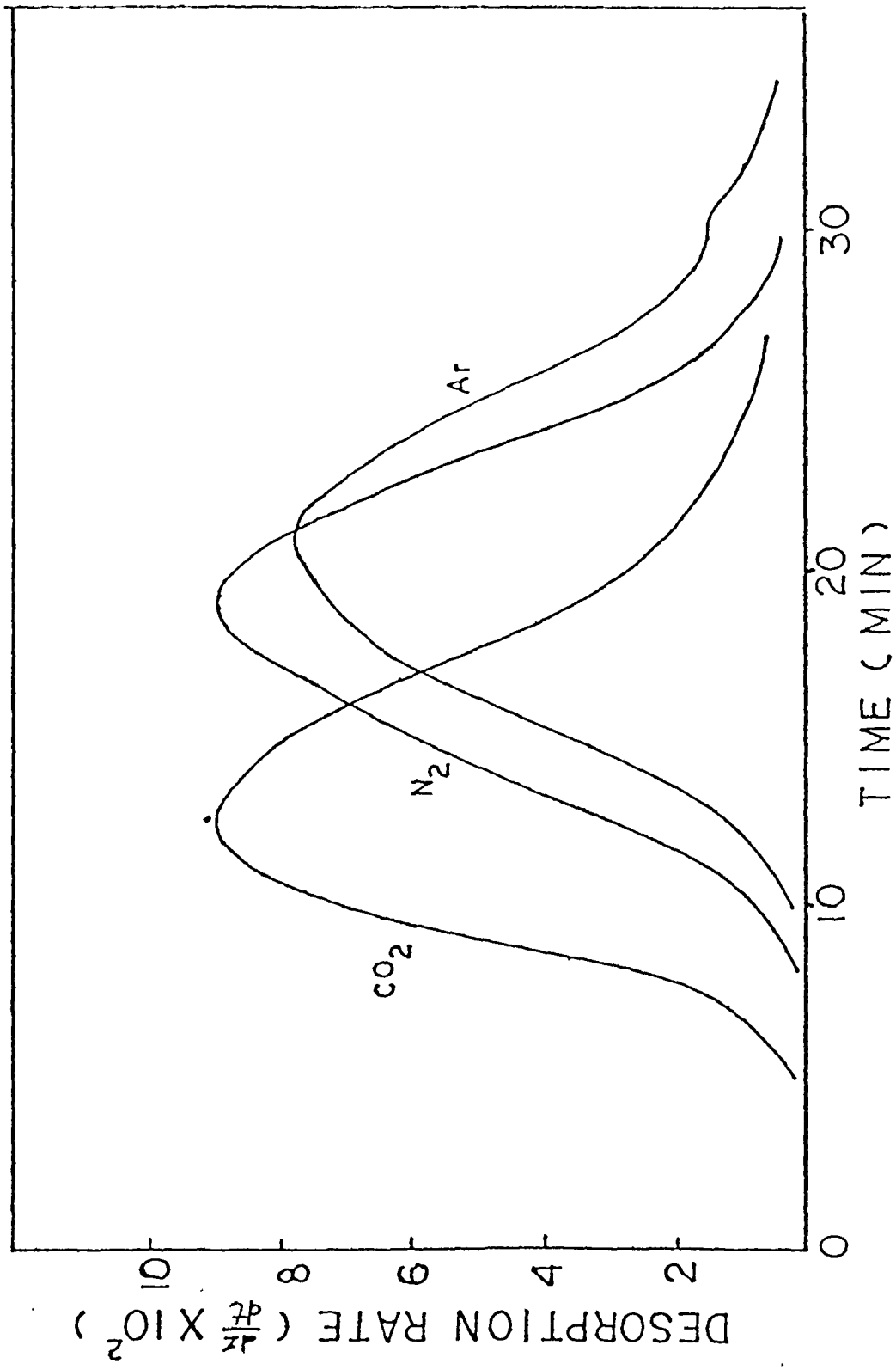

FIG. 4.1 TYPICAL TPD SPECTRA AT A HEATING RATE OF 17°C / MIN.

Table 4.1

Encapsulation in 3A

Gas	Temperature (°C)	Pressure (psig)	Volume Trapped (c.c.STP/g) Volumetric	TPD
N_2	350	1800	45	47
Ar	350	1750	46	45
CO_2	350	800	78	76

Table 4.2

Size of Molecules

Gas	Pauling's Dimension (Å)	Kinetic Diameter σ (Å)	r_m (Å)	Diameter* (Å)
N_2	4.1 X 3	3.64	4.09	3.86
Ar	3.84	3.4	3.84	3.63
CO_2	5.1 X 3.7	3.3	-	3.9

r_m is the intermolecular distance at which minimum potential energy occurs.

σ is the collision diameter - the intermolecular distance of closest approach for two molecules colliding with zero initial kinetic energy.

* based on molecular volume at the boiling point.

depends on the size of molecule, more Ar would be trapped since the kinetic diameter of Ar (3.4 Å) is smaller than that of N_2 (3.64 Å), as shown in Table 4.2. However, the nitrogen molecule is elongated and according to Pauling the dimension is 4.1 X 3.0 Å while Ar is spherical with a diameter of 3.84 Å. It is possible that the linear molecule of N_2 could enter the apertures of the zeolites longitudinally. The fact that N_2 is not adsorbed by 3A at -78°C indicates that the effective diameter of N_2 is larger than 3 Å. Considering the molecular volume of the gases at their boiling points (Table 4.3), with that of CO_2 obtained by extrapolating the reciprocal volume of CO_2(liquid) to -78°C, the molecular diameters were calculated assuming the molecules are packed in compact forms. N_2 has a diameter of 3.86 Å, larger than that of Ar (3.63 Å) but smaller than that of CO_2(3.9 Å). Thus, the high trapping capacity for CO_2 could be due to the electronic nature of the molecules. The ionic surface of the zeolite has a strong affinity for CO_2 and N_2 whose quadrupole moment may interact with the electric field inside the structure. The quadrupole moment for non-rotating N_2 and CO_2 molecules are 2.5 X 10^{-26} (e.s.u.) and 8.2 X 10^{-26}(e.s.u.) respectively(22, 23). The fact that CO_2 boils at a higher temperature also increases adsorption.

Under the conditions of the encapsulation the amount of gas that can be stored in the void space (0.27 c.c./g) of the sieve, accounting for non-ideality of gas, is about 30 c.c.(S.T.P.)/g for Ar and N_2, and 13 c.c.(S.T.P.)/g for

CO_2. It is difficult to distinguish whether the molecule is adsorbed or not in a cavity of diameter only three times that of the molecule. The Polanyi theory (39) predicts for 4A zeolite (vapour pressure of adsorbate being extrapolated beyond the critical point) about 11 % of the void volume would be saturated with the adsorbate in liquid form at the encapsulation conditions, and about 3 % at room temperature and atmospheric pressure. Thus, most of the trapped gas would be in the gaseous state. The number of molecules trapped per unit cell is about 3 for Ar and N_2 , and about 6 for CO_2.

The trapped gas molecules may vibrate with many possible frequencies in any cavity. The energy of binding an Ar molecule within the interstices of the β-cage was calculated by Barrer(10) using Leonard Jones 12-6 Potential. The calculation was based on the dispersive and repulsive forces between the gas molecules and the framework oxygen anions and the gas molecules . The value of activation energy obtained is low (6 kcal/mole) compared with the experimental value (19 kcal/mole). For CO_2 and N_2 , the calculation would involve the polarization energy in addition to the dispersive and repulsive energy.

Fig. 4.2 shows a plot of the amount of gases remaining as a function of time. The different slopes indicate the different rate of leaking. The data show that CO_2 leaked much faster than N_2 and Ar. About 20 c.c.S.T.P./g leaked in the first 30 days for CO_2 , and less than 5 c.c.S.T.P./g for N_2 and Ar.

FIG 4.2 VOLUME OF GAS VS TIME $^{1/2}$

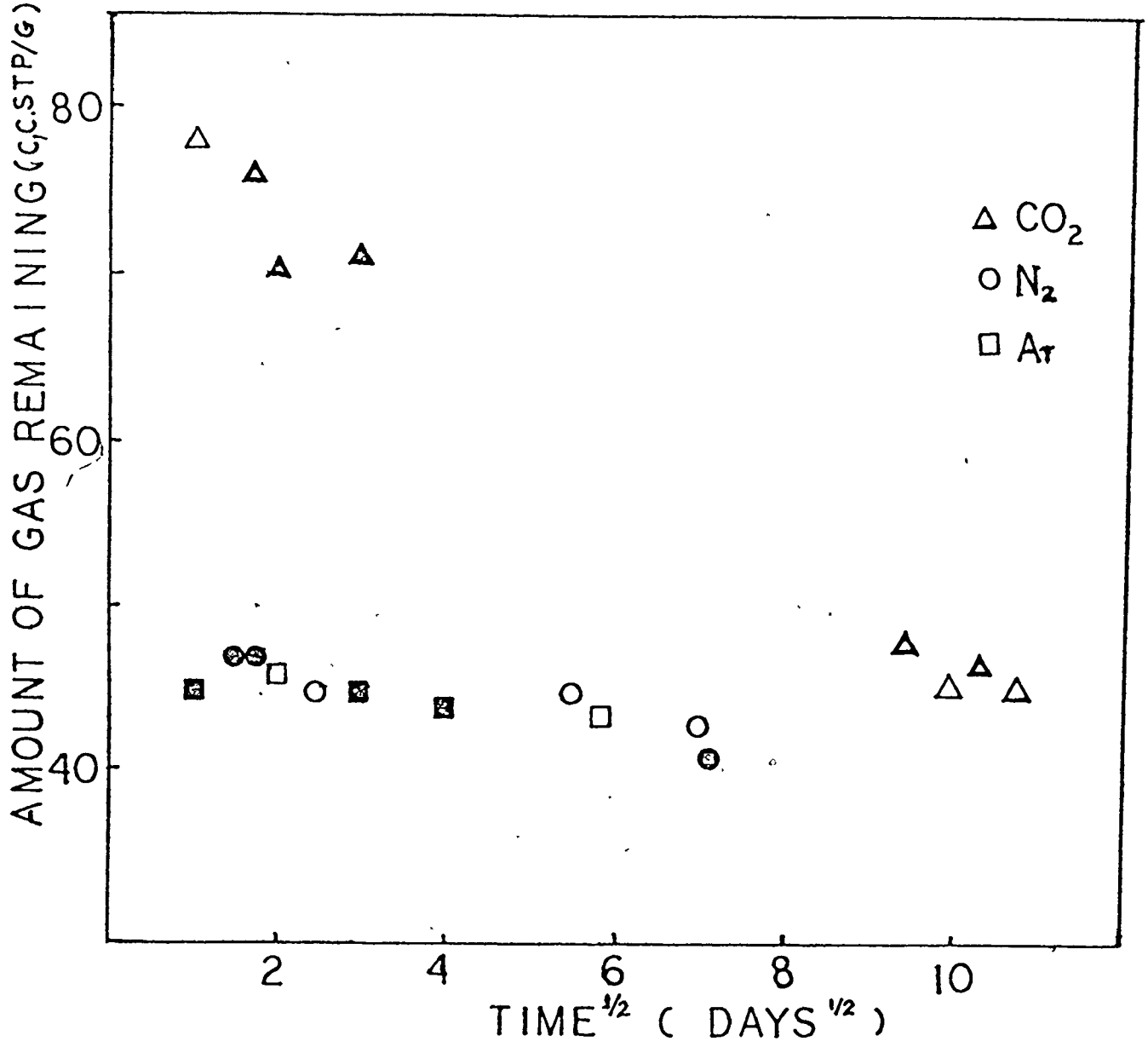

Note: Solid symbols represent TPD data;

Open symbols represent Volumetric data.

4.2 Kinetics

Consider first of all the diffusion-controlled kinetics based on Fick's Second Law of diffusion for uniform sized particles. Fig. 4.3 shows a typical plot of ln k against 1/T , where k is expressed in terms of the rate, $\frac{dZ}{dt}$ and the fraction of gas desorbed, Z, as given by equation (13). If the equation holds, a straight line would be obtained. The graph shows that a straight line can be drawn passing through the first set of data points from room temperature up to about 200°C. The gradient of the slope gives a value of -16×10^3 and hence the activation energy is 32 kcal/mole and k_o is 10^9 per minute. However, if one considers the range of temperature from 200°C to 400°C, the slope of the straight line gives an activation energy of 17 kcal/mole and k_o equal to 10^4 per minute. The slope of the curve at any point after 400°C changes to a positive value.

The reason that equation (13) does not represent the data properly is that the assumption of uniform sized particles does not hold. From the definition of $k_o = D_o/a^2$, where a is the length of half-side of a cubic particle, and the fact that by the time the desorption process reaches 400°C, most of the gas in smaller particles would be depleted, leaving only the large particles, the value of k_o becomes smaller accordingly. In the Arrhenius plot, if the deviations of the experimental data from the straight line were plotted against the absolute temperature, a straight line was obtained showing that k is not a constant but a function of temperature. Fig. 4.4 shows that k_o decreases exponentially with temperature, $k_o = k''\exp(-.029T)$. If this expression is built into equation (13), the data are represented reasonably well.

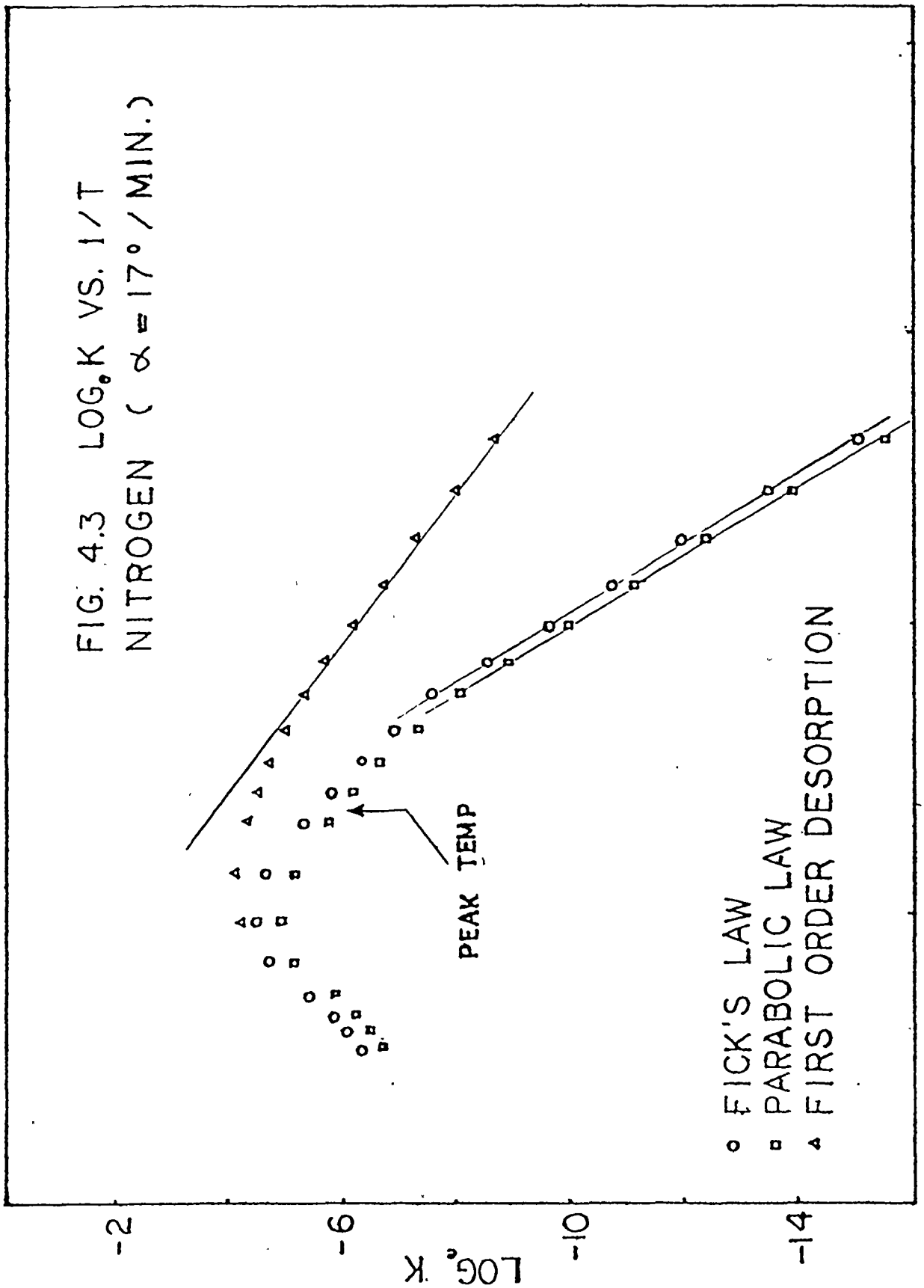
FIG. 4.3 LOG$_e$K VS. 1/T
NITROGEN (α = 17° / MIN.)
LOG$_e$ K
10^3 / T (°K)
-2
-6
-10
-14
1.0
1.5
2.0
2.5
3.0
PEAK TEMP
FICK'S LAW
PARABOLIC LAW
FIRST ORDER DESORPTION

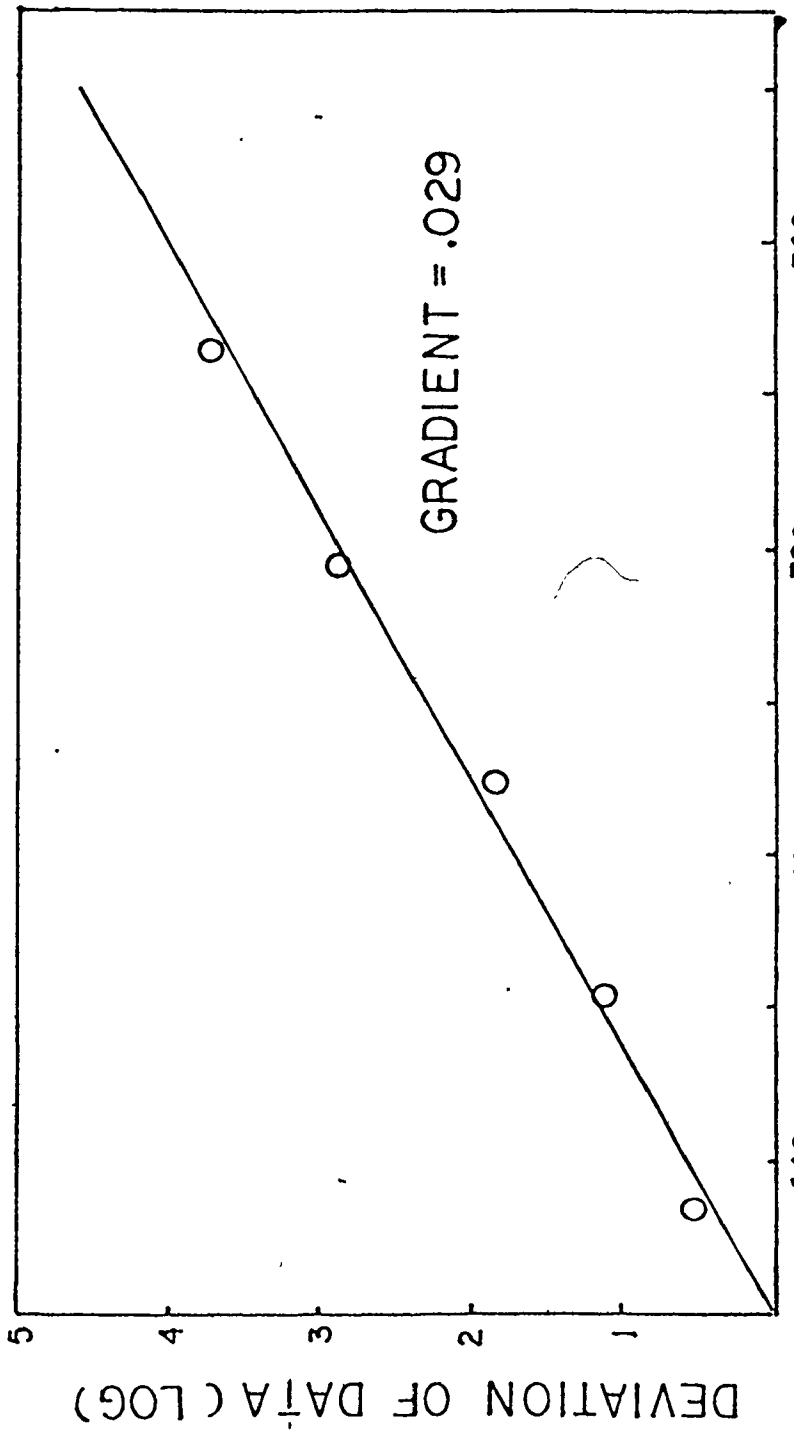

Figure 4.4 Plot of the Deviations of Experimental Data versus Temperature

The Parabolic Law predicts the same activation energy for diffusion as the diffusion-controlled kinetics, as shown in Fig. 4.3, for the low temperature range. The diffusivity predicted will be smaller than that predicted by diffusion-controlled kinetics because of a smaller value of pre-exponential factor. Apparently the failure of Parabolic Law is also due to the variation of particle sizes. Referring to Section 3.8, the results of the adsorption data of nitrogen on the desorbed samples do not justify the assumption that the apertures are permanently enlarged.

For first order desorption kinetics, the plot of equation (17) is presented in Fig. 4.3 . It also does not give a straight line except the initial part of the curve. However, the plot of the desorption-controlled equation coincides with that of the diffusion-controlled equation at the end of the desorption ($Z > .83$). The activation energy for desorption estimated from the initial part of the curve turns out to be the same value (about 17 kcal/mole) as the activation energy for diffusion in the range of temperature from 200°C to 400°C.

The first order desorption kinetics is derived for a plane surface. No size distribution is involved in the assumption. The curvature in the Arrhenius plot indicates that the first order kinetics does not hold. Therefore, none of the equations fit the data except for a limited range of temperature. In the following discussions Fick's Law solution is modified to include the effect of particle size distribution.

The correct choice of particle geometry is important in analysing rate data. Solutions for Fick's Law for diffusion into an infinite platelet, a sphere and a cube are given in Table 2.1 (Chapter 2). In analogy to heat conduction problems the simplified equations for the cube were obtained by cubing the platelet solution (37). Comparing equation (14) and (12) shows that the rate of diffusion for cubes is 25 % slower than that for spheres for $\tau > .16$. The difference in rate for $\tau < .16$ is negligible. Hence, all calculations in this work are based on equations for cubes so that the shape factor can be taken into account though the cubic particles of sizes larger than 2 microns have their corners chopped off (Fig. 3.12).

An approximate value of the activation energy for diffusion can be estimated from the location of the peak maximum of the desorption spectrum. The relation between the peak temperature and the heating rate is developed for Fick's Law solution. Differentiating the rate expressions (13) and (14) with respect to time, and setting $\frac{d^2Z}{dt^2} = 0$, the conditions at the peak maximum for cubic particles are as follows:

For $0 < Z_m < .83$,

$$T_m^2/\alpha = 3\ E/\left\{ R \left(\frac{dZ}{dt}\right)_m \left(2/(1-Z_m) + (1-Z_m)^{-2/3}/(1-(1-Z_m)^{1/3}) \right)\right\}$$

For $1 > Z_m > .83$,

$$T_m^2/\alpha = E\ (1-Z_m)/\left(R \left(\frac{dZ}{dt}\right)_m \right)$$

Hence, from a knowledge of T_m, α, Z_m and $\left(\frac{dZ}{dt}\right)_m$, the activation energy, E, can be calculated. This only gives an estimate of

the activation energy since uniform sized particles are assumed in the derivation of equation (13) and (14).

The theoretical model (Section 2.4) based on the series solutions to Fick's Second Law of diffusion taking into account the size distribution and the shape of particles seems to be able to fit the experimental data for the entire range of temperature. A simplified form of equation (37) is used, which saves a lot of computer time since the number of calculations is reduced by a factor of n^2, where n is the terms included in the series solutions. The series solution converges well for $\tau > .16$, but it is difficult to converge for $\tau < .16$ even if a large number of terms is included. In the present computer program the number of terms used is 20.

The effect of using a constant particle size (the weight average) is shown in Fig. 4.5. Comparing with the experimental curve, the predicted rate is smaller at the start as well as at the end of desorption. The peak maximum occurs at about the same time but with a higher rate. The slope of the curve is distorted, less symmetrical than the experimental data. The shape can be predicted fairly accurately using the theoretical model.

Table 4.3 gives the parameters for diffusivity of the various gases in zeolite 3A. The parameters were determined by fitting the experimental data to the theoretical model, which takes into consideration the effect of the shape and size distribution of the particles, using nonlinear regression analysis. The computer subroutine used for regression is Subroutine UNHAUS. The initial guesses for the parameters

Figure 4.5

Test of Fick's Law solutions for N_2 at a heating rate of 17 C/min.

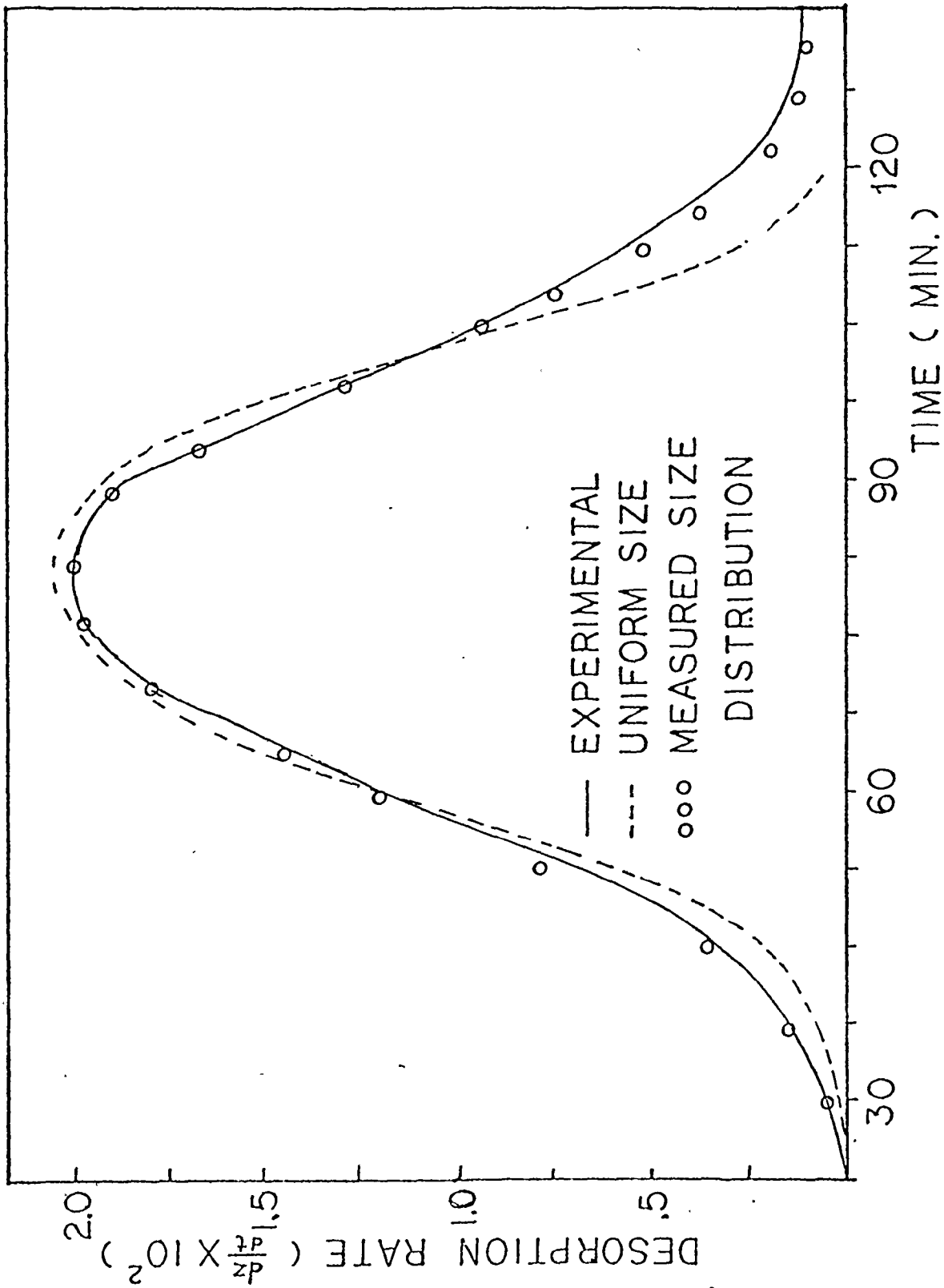
DESORPTION RATE ($\frac{dz}{dt} \times 10^2$)
2.0
1.5
1.0
.5
30
60
90
120
TIME (MIN.)
EXPERIMENTAL
UNIFORM SIZE
MEASURED SIZE
DISTRIBUTION

Table 4.3

Diffusivity Coeffients ($D = D_o \exp(-E/RT)$)

of N_2 , CO_2 and Ar in Zeolite 3A

Gas	$D_o X 10^5$ (cm^2/sec)	E (kcal/mole)	$D_{298°K} X 10^{18}$ (cm^2/sec)
N_2	2.174 ± .138	17.34 ± .49	4.18
CO_2	.143 ± .021	13.04 ± .70	390.5
Ar	.303 ± .030	15.84 ± .82	7.32

were estimated by plotting the data as shown in Fig.4.3, or by using the peak temperature-heating rate relationship. Least square method was used in the nonlinear parameter estimation. The sum of squares of residues, the difference between the measured and calculated values, was minimized. There is a high correlation between the two parameters, D_o and E. The parameters are reparameterized such that the expression for D becomes

$$D = D' \exp\left(-\frac{E}{R}\left(\frac{1}{T} - \frac{1}{T_c}\right)\right)$$

where $D' = D \exp(E/RT)$

T_c = average temperature, K.

The confidence limits of the parameters at 95 % confidence level were calculated. The diffusivities calculated at room temperature show that CO_2 has a much higher value than Ar and N_2 .

Fig. 4.6 shows the experimental data of nitrogen at different heating rates and the theoretical model fitted by two parameters D_o and E. The same parameters are used for each heating rate and there is good agreement between the theoretical and experimental data. The data for carbon dioxide is not very well predicted by the model (Fig. 4.7). The variance of residues for N_2 is of the order of 10^{-6} and that of CO_2 is 10^{-5}. It is possible that the diffusivity of carbon dioxide in 3A is concentration dependent. The large leak rate may affect the initial distribution of gas within the particle which should be uniform in order that the solution for Fick's Law applies.

The TPD spectra for argon was fitted to the model by four parameters. It was postulated that the gas evolved

Figure 4.6

Desorption Spectra for Nitrogen at Different Heating Rates. Solid curves are experimental and symbols give calculated data.

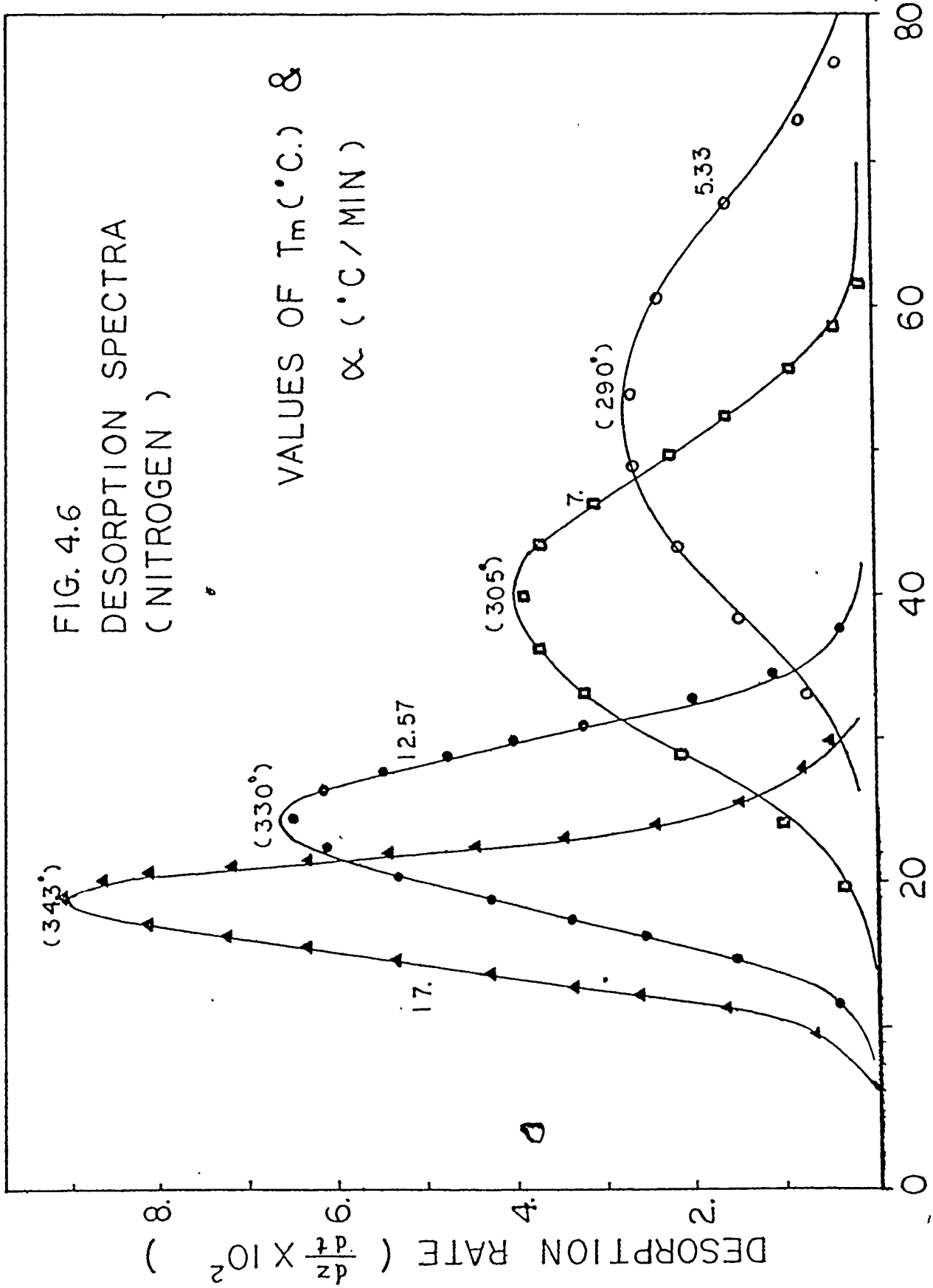
FIG. 4.6
DESORPTION SPECTRA
(NITROGEN)
VALUES OF T_m (°C.) &
α (°C/MIN)
(343°)
(330°)
(305°)
(290°)
12.57
7.
5.33
17.
DESORPTION RATE ($\frac{dz}{dt} \times 10^2$)
TIME (MIN.)
0
20
40
60
80
2.
4.
6.
8.

Figure 4.7

Desorption Spectra for Carbon Dioxide at different Heating Rates. Solid curves are experimental and symbols give calculated data.

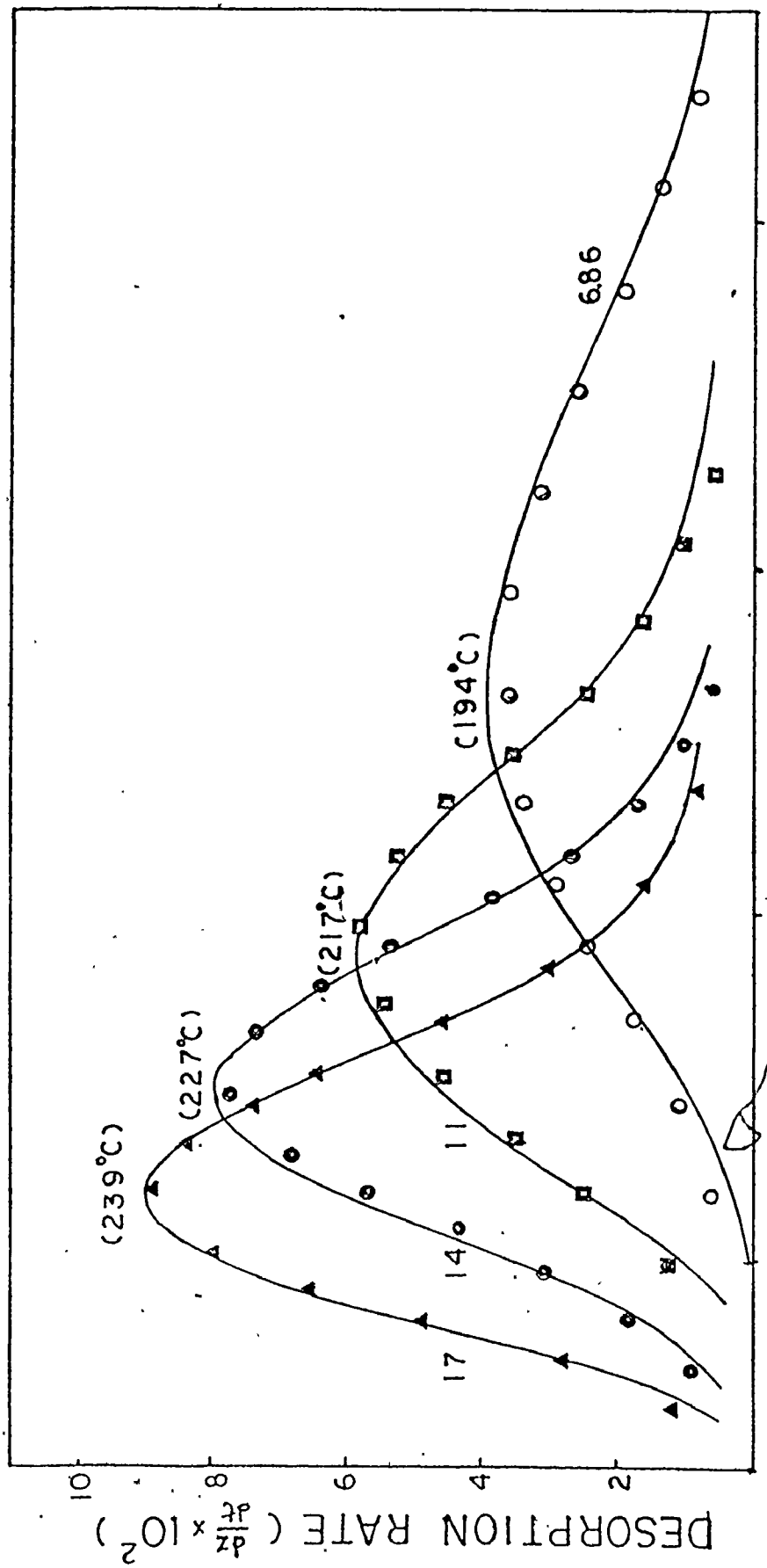

FIG-4.8 DESORPTION SPECTRA OF CARBON DIOXIDE AT DIFFERENT HEATING RATES

at 500°C comes from the β-cages as well as the α-cages. The responses measured would be the resultant rate of gases desorbed from the two structures. The gas from the α-cages should be desorbed at a lower temperature than that from the β-cages.

Let Q_T be the total amount of gas desorbed, Q_α be the amount desorbed from structure α and Q_β be the amount from structure β. Then

$$\frac{dQ_T}{dt} = \frac{dQ_\beta}{dt} + \frac{dQ_\alpha}{dt}$$

$$\text{and} \quad \frac{dZ}{dt} = F\,\frac{dZ_\beta}{dt} + (1 - F)\,\frac{dZ_\alpha}{dt}$$

where F is the fraction of gas in β structures. In the present case 16 % was assumed to be the fraction of gas trapped in β cage, which is the volume fraction of β-cages in a unit cell.

The small peak at 500°C is not very sensitive to regression analysis because of the very small contribution to the variance of residues. Resulting parameters are highly correlated. The diffusivities were found by trial and error method to be $D_\alpha = 3.83 \times 10^{-6} \exp(-16000/RT)$ and

$$D_\beta = 1.32 \times 10^{-6} \exp(-18000/RT)$$

In fact, β-cages are enveloped by α-cages in the three dimensional structure of the zeolite. Only at high temperatures can the trapped molecules in β-cages overcome the energy barrier and go into the α-cages where the molecules can be desorbed more readily through the 3 Å apertures. If the small amount of gas released at 500°C was ignored, the two-parameter model is a good approximation to the real curve as shown in Fig. 4.8 .

Figure 4.8

Desorption Spectra for Argon at Different Heating Rates. Solid curves are experimental and symbols are calculated data.

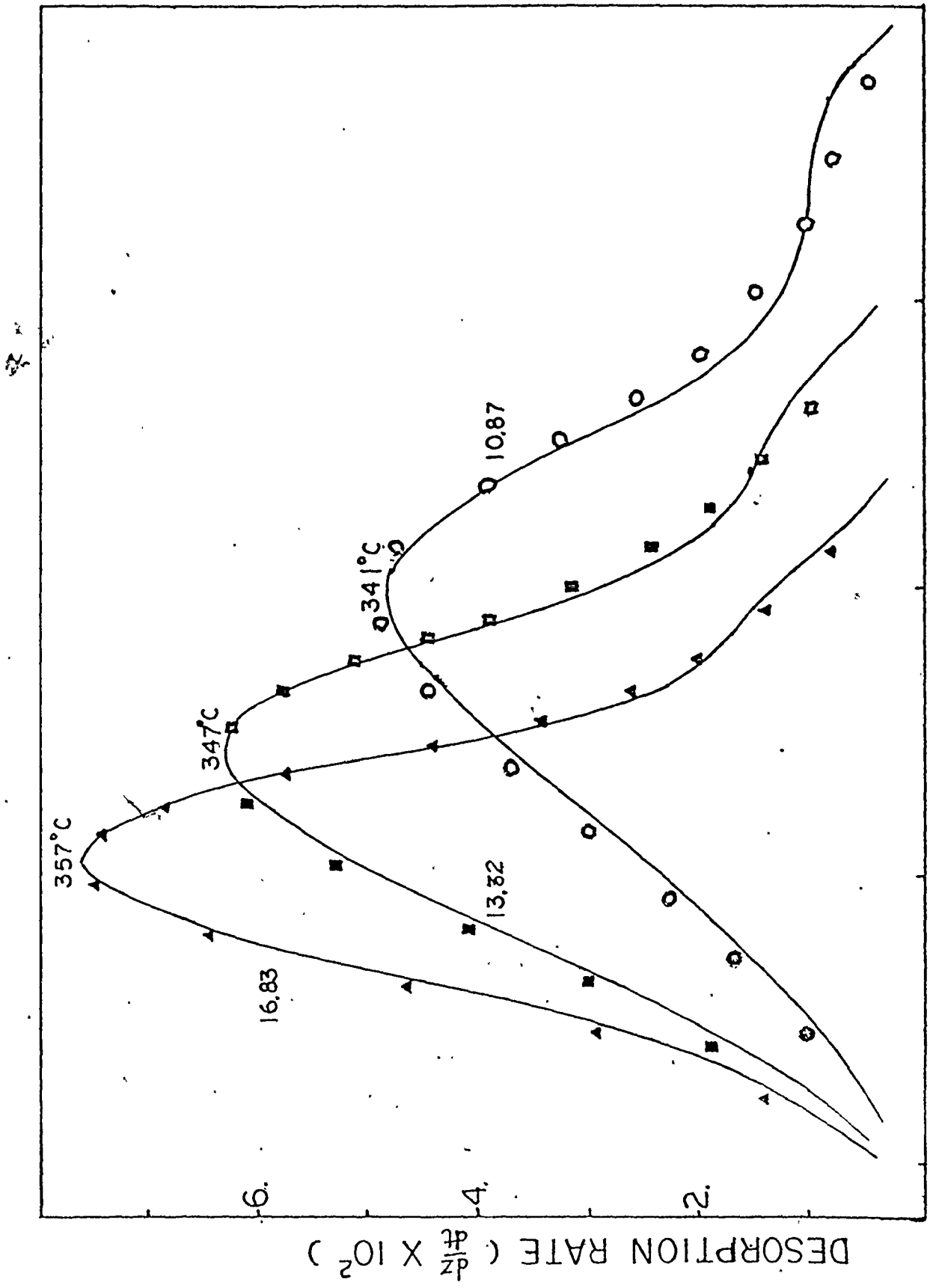
DESORPTION RATE ($\frac{dz}{dt}$ X 10^2)
TIME (MIN)
357°C
347°C
341°C
16.83
13.82
10.87
2
4
6
10
20
30
40

Comparing the diffusivities calculated with literature data, activation energy for Ar is 2 kcal/mole higher than that given by Nelson (14), and for N_2 about 1 kcal/mole, whereas for CO_2 , the value exceeds the literature data (41) by 9 kcal per mole. The difference could be due to the different amount of gas trapped in the sieve and that the diffusivity, D is concentration dependent. Also the type of sieve used in the present analysis is 50 % potassium exchanged NaA zeolite.

In the present analysis, no investigation was made on the dependence of diffusivities on the amount trapped. The results presented refer to experiments conducted in a period of two to three weeks during which the change of initial amount due to leakage is not significant for argon and nitrogen. As the volume of trapped gas at 2000 psig. is far from the saturation value (which should be larger than that trapped at 2000 atmosperes, 100 c.c.S.T.P./g), the isotherm of encapsulation is expected to be linear in the range of 1 to 150 atmospheres so that the effect of concentration dependence on diffusivity is small. If the driving force for diffusion is chemical potential, rather than concentration gradient, the expression for diffusivity at a constant temperature (40) is

$$D = \frac{R\,T}{\kappa} \frac{d \ln p}{d \ln c}$$

Since the derivative d(ln p)/d(ln c) is unity for linear isotherm and κ is a constant independent of concentration, the diffusivity is only a function of temperature.

Fig. 4.9 shows the TPD spectra for desorption of argon in the presence of water vapour. Water vapour at room temperature (21 torr at 23°C) was added continuously and intermittenly to the carrier gas stream. A dry-ice trap was used to remove water vapour from the output stream so that only the concentration of the desorbed gas was detected by the thermal conductivity cell. The carrier gas flowrate remained the same and the base line of the recorder was unchanged. For continuous addition of water vapour, the small peak at 500°C that is usually present in the case of dry carrier gas disappeared. Instead, a relatively large peak appeared at about 200°C in addition to the peak at 350°C. Progressive adsorption of water vapour occurs up to some temperature (about 250°C) and above this temperature desorption of water vapour is favoured.

Comparing the two spectra (with and without water vapour) the disappearance of the second peak may indicate the gas from β-cages was released at a lower temperature owing to the addition of water vapour. Water molecules and argon are desorbed simultaneously for temperatures above 350°C.

Fig. 4.10 shows the effect of intermittent addition of water vapour on desorption of Ar at several constant temperatures. In this intermittent experiment, the increase in temperature was about 1°C. due to the heat of adsorption of water on the sample. At a temperature of 200°C, for example, the increase in rate due to the increase in temperature would only be 3 % (E = 15840 cal/mole) assuming the Arrhenius dependence of temperature for rate. The observed increase in rate was 90 %.

Figure 4.9
The Desorption Spectra of Argon
in the Presence of Water Vapour
at a Heating Rate of about 17°C/min.
The Curve with dotted lines represent
the spectrum of Ar without water at
the same heating rate.

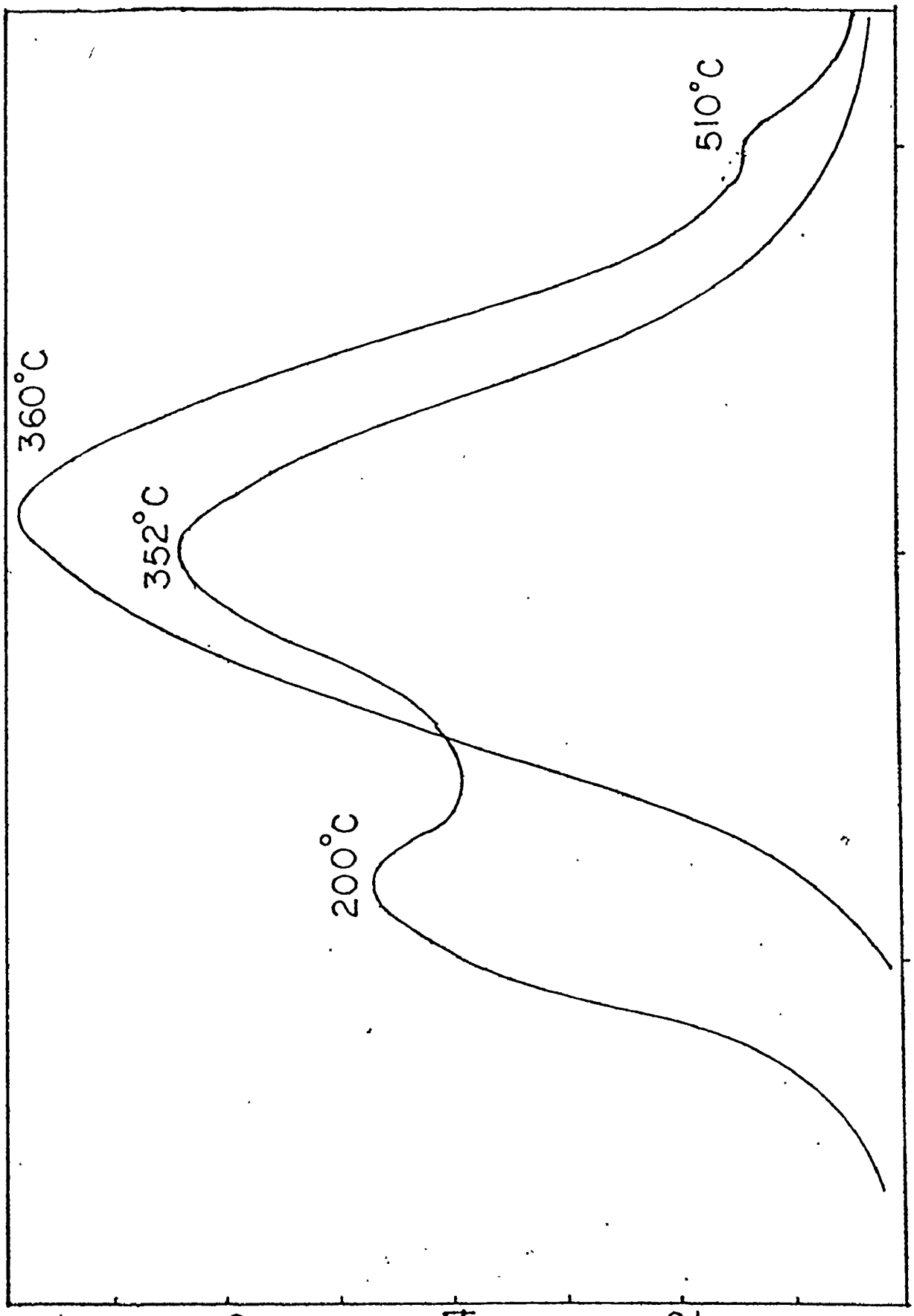
360°C
352°C
200°C
510°C
DESORPTION RATE ($\frac{dz}{dt}$ X 10⁷)
TIME (MIN)
2
4
6
10
20
30

Figure 4.10
Diagram of the Signal Response
for intermittent water addition experiments
at constant temperature.

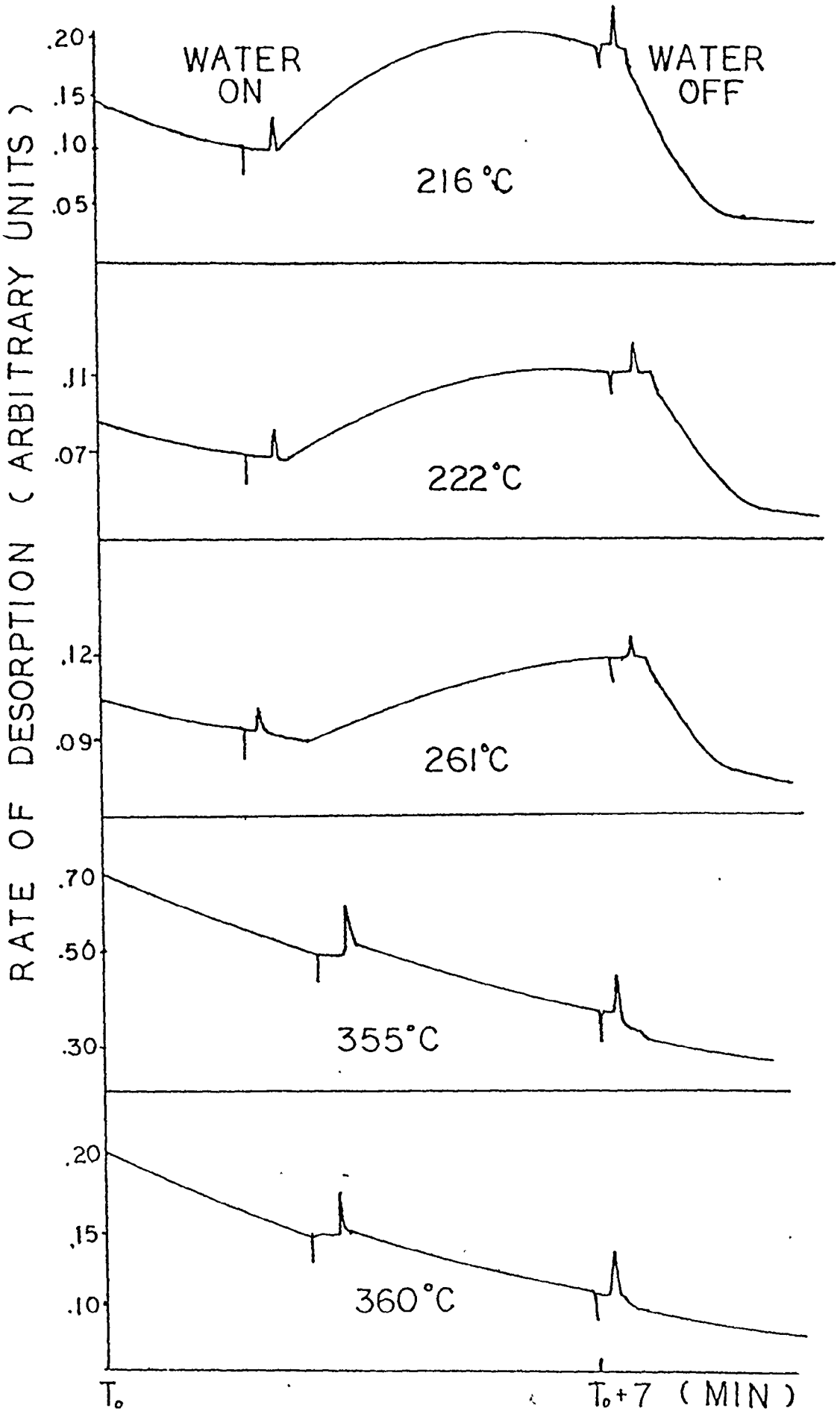
RATE OF DESORPTION (ARBITRARY UNITS)
.20
.15
.10
.05
WATER ON
WATER OFF
216 °C
.11
.07
222°C
.12
.09
261°C
.70
.50
.30
355°C
.20
.15
.10
360°C
T₀
T₀+7 (MIN)

Thus, the enhanced rate is due to other factors than the effect of temperature.

During the adsorption of water vapour, the cations K^+ and Na^+ may be hydrated and become mobile in the cavities. The positions of the potassium ions that regulate the openings of the pores might be displaced by the presence of water molecules, and effectively lower the activation energy for diffusion of the adsorbate. Also, at low temperatures the water molecules may accumulate and occupy most of the void space of the cavities displacing the trapped gas molecules from the cavities. There was no significant change in rate of desorption for temperatures above 350°C as the rate of adsorption of water vapour is negligible at high temperature. The results seem to indicate that the presence of water vapour during desorption decreases the activation energy for diffusion of the trapped gas through the apertures connecting the α-cages as well as those connecting the α-cages and β-cages though there is no confirmative evidence that any gas was trapped inside the β-cage.

CHAPTER 5

CONCLUSIONS

Fick's Second Law of diffusion, applied to temperature programmed desorption with a linear temperature schedule, is able to describe satisfactorily the kinetics of the release of trapped gases (N_2 , Ar and CO_2) in 3A Zeolite, if the cubic shape of the particles and the size distribution are considered. Equations for constant particle size are inappropiate. Water vapour enhances the desorption rate of the trapped gases.

BIBLIOGRAPHY

1. Barrer, R.M., J. Chem. Soc., 2158 (1948).
2. Barrer, R.M., Discussions Faraday Soc., 40, 206 (1944).
3. Barrer, R.M., Trans. Faraday Soc. 45, 358 (1949).
4. Barrer, R.M., Brit. Chem. Eng. 4, 267 (1959).
5. Eagan, J.D., Ph.D. Thesis, McMaster University (1972).
6. Cvetanovic, R.J., and Amenomiya, Y., Advan. Catal. 17, 103 (1967).
7. Reed, T.B., and Breck, D.W., J. Amer. Chem. Soc. 78, 5972 (1956).
8. Yanagida, R.Y., Amaro, A.A., and Seff, K., J. Phys. Chem. 77, 805 (1973).
9. Leung, P.C.W., Kunz, K.B., Seff, K., J. Phys. Chem. 79, No. 20, 2157 (1975).
10. Barrer, R.M., and Vaughan, D.E.W., Surface Science 14, 77 (1969).
11. Barrer, R.M., and Vaughan, D.E.W., Trans. Faraday Soc. 63, 2275 (1967).
12. Barrer, R.M., and Vaughan, D.E.W., J. Phys. Chem. Solids 32, 731 (1971).
13. Breck, D.W., J. Chem. Educ. 41, 678 (1964).
14. Nelson, E.T., and Walker, jun. P.L., J. Appl. Chem. 11, 358 (1961).
15. Grant, W.A., and Carter, G., Vacuum 15, No. 10, 477 (1965).
16. Farrell, C., Grant, W.A., Erents, K., and Carter, G., Vacuum 16, No. 6, 295 (1966).

17. Smutzek, M., Cerny, S., and Buzek, F., J. Catal. 24, 343 (1975).

18. Barrer, R.M., and Rees, L.V., Trans. Faraday Soc. 50, 853 (1954).

19. Breck, D.W., Eversole, W.G., Milton, R.M., Reed, T.B., and Thomas, T.L., J. Amer. Chem. Soc. 78, 5963 (1956).

20. Habgood, H.W., Can. J. Chem. 36, 1384 (1958).

21. Ruthven, D.M., and Loughlin, K.F., Chem. Eng. Science 26, 577 (1971).

22. Eagan, J.D., and Anderson, R.B., J. Colloid Interfac. Sci. 50, No. 3, 419 (1975).

23. Crank, J., The Mathematics of Diffusion. Clarendon Press, Oxford (1956).

24. Weisz, P.B., and Goodwin, R.D., J. Catal. 2, 397 (1963).

25. Stifel, G., Master's Thesis, McMaster University (1966).

26. Irani, R.R., and Callis, C.F., Particle Size Measurement, Interpretation, and Application, Wiley, New York (1963).

27. Beckmann, P., Elements of Applied Probability Theory, Harcourt, Brace & World, Inc. (1967).

28. Pickering, W.F., Modern Analytical Chemistry, Marcel Dekker, Inc., New York (1971).

29. Woolfson, M.M., An Introduction to X-ray Crystallography, Cambridge University Press (1970).

30. Milton, R.M., U.S. Pat. 2,882,243 (1959).

31. Breck, D.W., Eversole, W.G., Milton, R.M., Reed, T.B., and Thomas, T.L., J. Amer. Chem. Soc. 78, 5963 (1956).

32. Smith, W.V., and Howard, R.R., Phys. Rev. 79, 132 (1950).

33. Buckingham, R.A., and Disch, R.L., Proc. R. Soc.,A, 273, 275 (1963).

34. McCalla, T.R., Introduction to Numerical Methods and Fortran Programming, J. Wiley & Sons, Inc. 1967.

35. Baver, et al, Proc. Symp. Appl. Maths., Vol. XV, Amer. Math. Soc. (1963).

36. Stroud, A.H.,and Secrest, D, Gaussian Quadrature Formulas, Prentice-Hall, Inc. (1966).

37. Carslaw, H.S. and Jaeger, J.C., Conduction of Heat in Solids, Oxford University Press, 1959.

38. Hilderbrand, F.B., Introduction to Numerical Analysis, McGraw-Hill Book Co., Inc. (1956).

39. Harper, R.J., Stifel, G.R., and Anderson, R.B., Can. J. Chem. 47, 4661 (1969).

40. Kreith, F., Principles of Heat Transfer, 2nd edition, International Textbook Co., Scranton (1965).

41. Walker, P.L., Austin, L.G., and Nandi, S.P., Chem. Phys. Carbon, 2, 257 (1966).

Appendix A-1 Glass Volume Measurements in Volumetric Apparatus

Appendix A-1.1

Determination of Void Volume in Gas Measuring System

The void volume is the volume of the capillary tubing of the apparatus (referring to Fig. 2.9 of Chapter 3)to the left of S2, below S1 and to the zero marks of the gas bulbs and burette, and mercury manometer. The glass bulbs and burette were maintained at 25°C by thermostatted circulating water. Keeping S2 closed, helium was admitted via S1 which was then closed. The number of moles of He admitted at pressure P and temperature T is

$$n = P (V_B + V_b + V_v) / RT$$

where V_B = volume of gas in burette,

V_b = volume of calibrated bulbs,

V_v = void volume

Rearranging the above equation we obtain

$$PV_B = - P(V_b + V_v) + nRT$$

A series of P and V_B readings are taken, and PV_B is plotted against P. Hence, from the slope of the graph V_v can be calculated as the volume of bulbs is known. Such a plot is shown in Fig. A1 . The volume V_v = 11.79 c.c. was used in calculating the volumetric data for all gases used.

FIG. A-1. HELIUM VOID SPACE PLOT

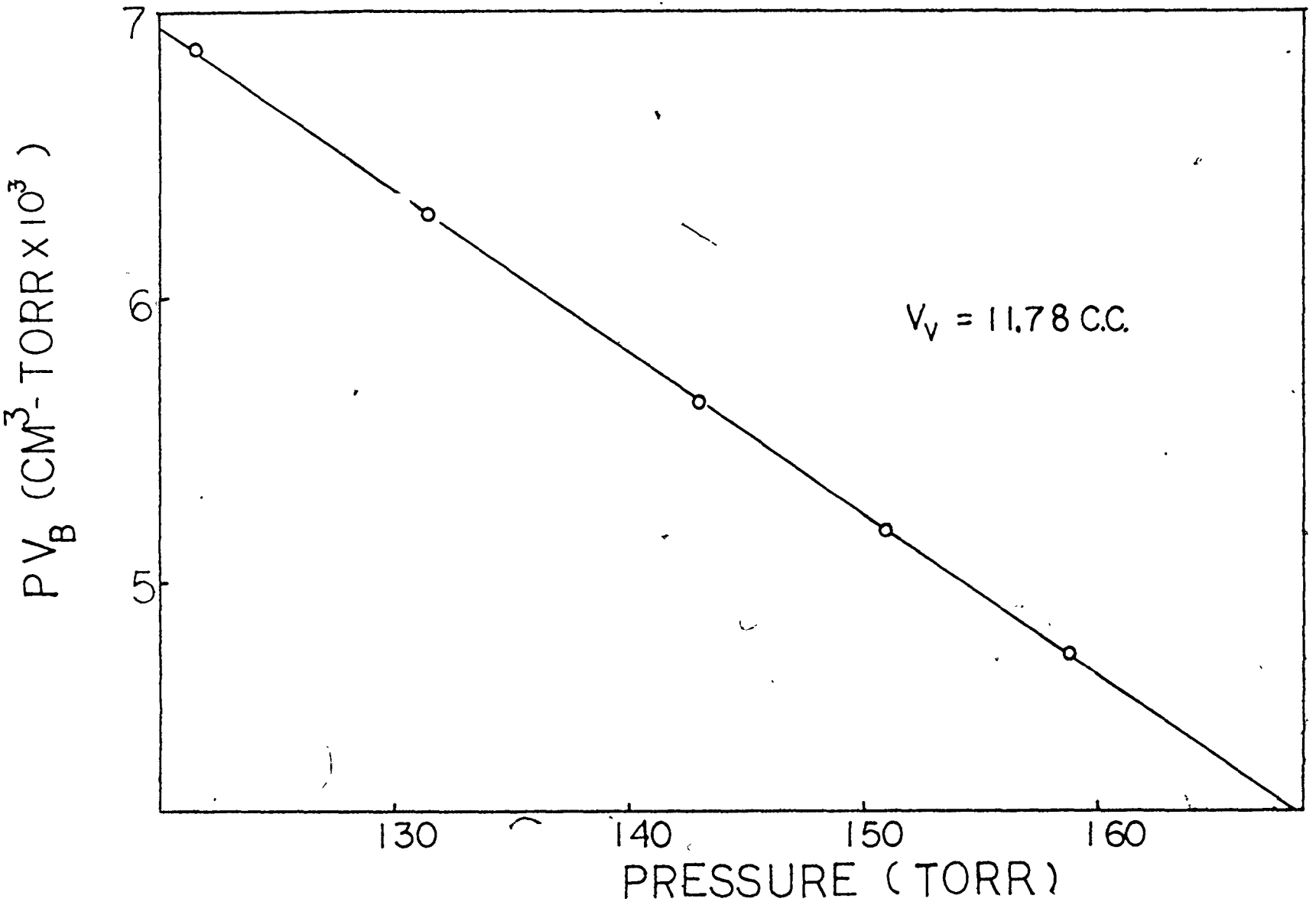

Appendix A-1.2

Dead Space Factor

The dead space factor F is defined as the number of c.c. at S.T.P. of gas per unit pressure which are present to the left of S2 (S3 open) but not adsorbed on the sample. F is a function of the temperature of the sample tube because the gas density changes and the sample tube volume changes slightly due to glass expansion/contraction. Helium was used for this determination because it is negligibly adsorbed on the zeolite sample even at liquid nitrogen temperatures. He was admitted via S1, with S2 closed. The inlet volume V_I (c.c. S.T.P.) can be calculated since V_v was determined to be 11.79c.c. A series of P and V_B readings were taken, with S2 being opened, to determine the volume V_R (c.c.S.T.P.) remained to the right of S2 at pressure P. The dead space factor is thus

$$F = (V_I - V_R)/ P$$

Let V_1 be the volume to the left of S2 at room temperature,

$V_2 = V_o + aT$ be the volume at the bath temperature,

where V_o is a constant and a is the coefficient of thermal expansion of glass (assumed constant over the range of T studied). Then

$$F = \frac{V_1(273)}{(760)\ T_R} + \frac{(V_o + aT)\ (273)}{(760)\ T}$$

or

$$F = A + B/T$$

where $A = (\frac{273}{760})(\frac{V_1}{T_R} + a)$ and $B = 273V_o/760$, both constant. Hence, plotting F against 1/T will give a straight line and a plot of F, determined for a series of sample tube bath temperature against 1/T is shown in Fig. A-2.

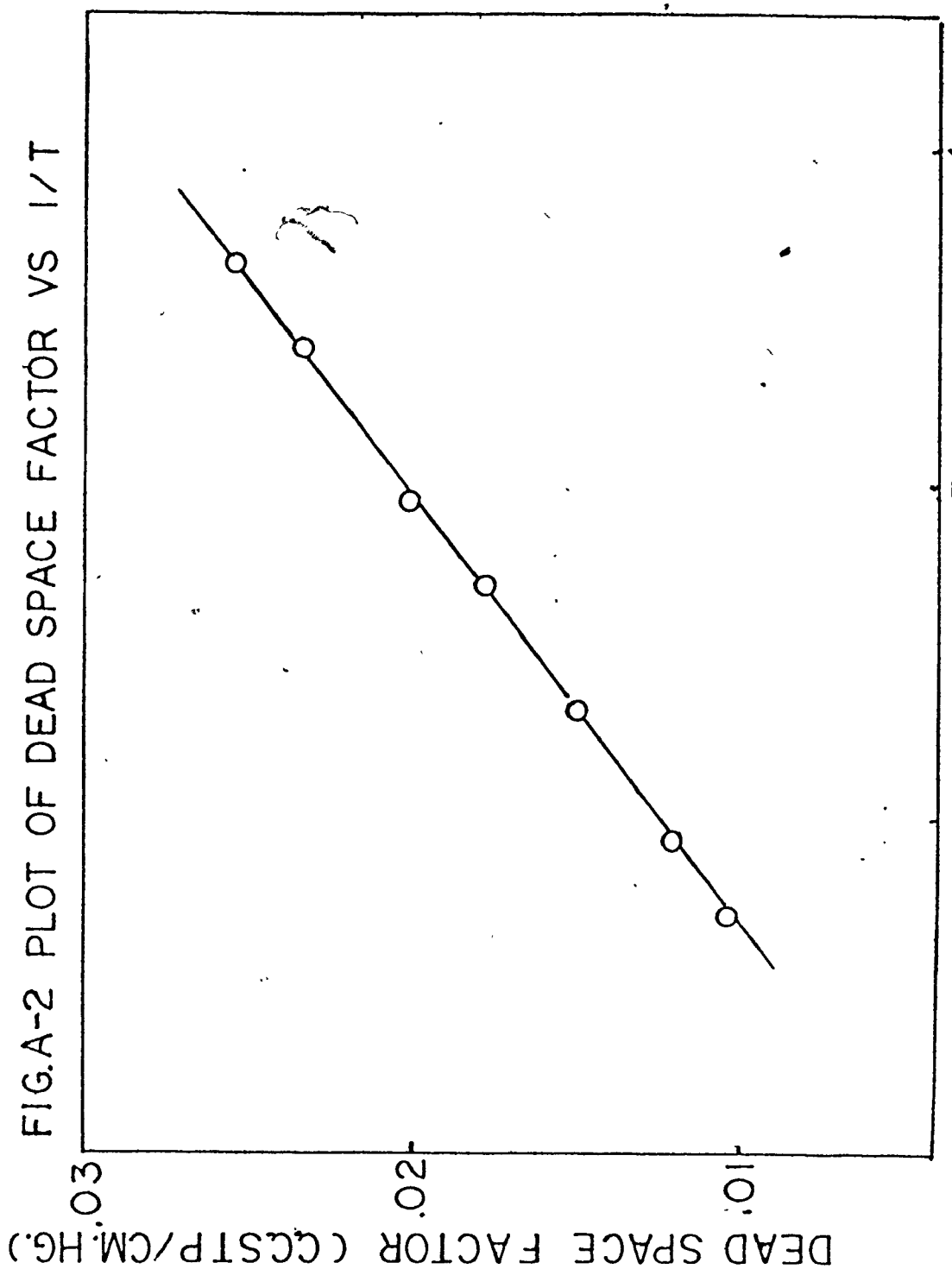
FIG.A-2 PLOT OF DEAD SPACE FACTOR VS 1/T
DEAD SPACE FACTOR (CCSTP/CM.HG.)
.03
.02
.01
2
3
4
RECIPROCAL TEMP. (X 10^{-3}K^{-1})

Appendix B1 Calibration of the Thermal Conductivity Detector

The interpretation of a temperature programmed desorption (T P D) spectrum required a correlation between concentration and signal response for hydrogen. A Varian Aerograph 6-port linear gas sampling valve was used to inject known volumes of gas into the carrier gas stream with sample loops of known volume. The amount of gas injected was corrected to S.T.P. conditions. The operating conditions of the detector cell are given in Table B. The recorded areas were measured by a disc integrator. The calibration was checked after each experiment was completed. Fig. B1 shows the linear response of the gases considered. The slope of the graph represents the calibration factor.

Table B1 Operating Conditions of the Thermal Conductivity Cell

1. Carrier gas - Helium
2. Pressure - Atmospheric
3. Filament Current - 200 mA
4. Detector Temperature - Room Temperature
5. Attenuation - Varible between 1 to 512
6. Flowrate - 40 ml/minute

FIG.B-I CALIBRATION OF DETECTOR RESPONSES FOR Ar, N_2 & CO_2

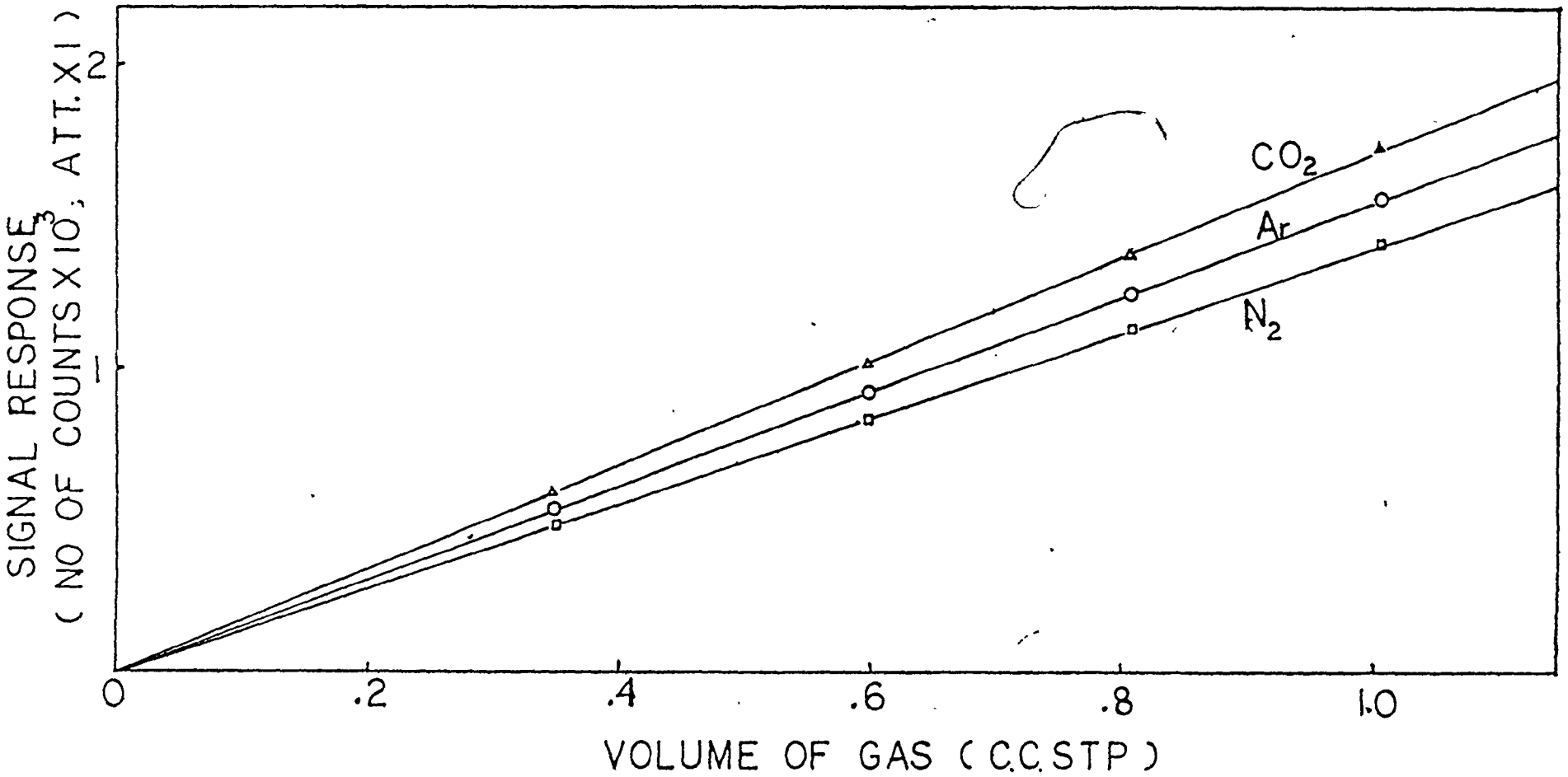

Appendix B2

Calibration of Flowmeter

FIG. B2
CALIBRATION OF FLOWMETER

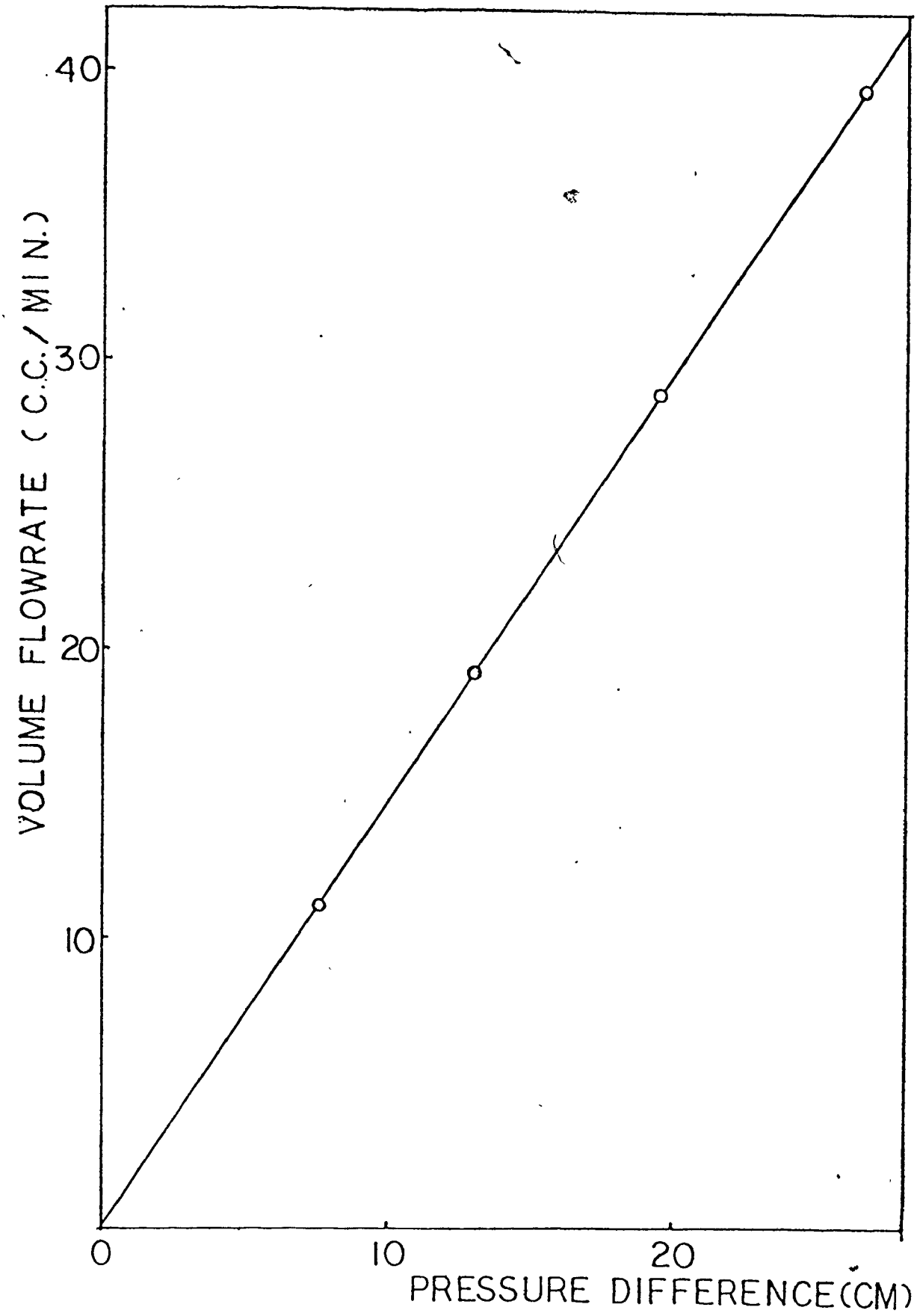

Appendix C-1 Comments On Computer Program Calculation

Referring to Section 2.4, Chapter 2, in calculating the rate $\frac{dZ}{dt}$, we have to evaluate τ . Letting $y = E/(R(T + \alpha t))$, the expression for τ can be transformed into

$$\tau = - \frac{D_o E}{\alpha R} \int_{y_o}^{y} \frac{\exp(- y) \, dy}{y^2}$$

where

$$y_o = E/RT$$

The solution for the integral is

$$= - \frac{DE}{\alpha R} \left\{ \frac{\exp(-y)}{y} + \ln y + \sum_{n=1}^{\infty} \frac{(-1)^n (y)^n}{n.n!} \right\}_{y_o}^{y}$$

However, the series solution does not converge for $y > 1$, and numerical integration has to be used to calculate τ . Subroutine TOR is used to find τ at any time t. The method employed is Romberg's method of numerical integration (34). This is a very efficient algorithm for the computation by digital computer of successive approximation of the definite integral $\int_a^b f(x)dx$. Trapezoid sums for the integral was computed using successively the intervals $h = b-a$, $h_1 = h_o/2$, $h_2 = h_o/2^2$,..., $h_k = h_o/2^k$. These areas were then interpolated to $h^2 = 0$ by applying repeated (iterated) linear interpolation in variable h^2, starting with points $(h_o^2 , A_o^o),\ldots,(h_k^2 , A_o^k)$, where the A_o^k are the trapezoid sum using interval h_k (k=0,1,...). The iterations stopped when the relative change of the value of the integral satisfied the tolerance ϵ or the interval h reaches a limit δ .

The integration of the rate of desorption over all particle sizes is based on Gaussian-Hermite Quadrature Integration Formula (38). For a continuous function f(x), integrated with the weighting function $w(x) = \exp(-x^2)$ over the interval $(-\infty, \infty)$, the integral is given by

$$\int_{-\infty}^{\infty} \exp(-x^2).f(x).dx = \sum_{k=1}^{n} H_k.f(x_k) + E$$

where x_i's are the roots of $H_m(x) = 0$

$$H_m(x) = (-1)^m.\exp(x^2).\frac{d^m}{dx^m}(\exp(-x^2))$$

$$H_i = \frac{2^{m+1}\ m!\sqrt{\pi}}{(H_{m+1}(x_i))^2}$$

and the error, $E = \frac{m!\sqrt{\pi}\ f^{(2m)}(\xi)}{2^m.(2m)!}$ for some ξ.

Tables for the values of the weighting factors H_i are available (36). For the Hermite polynomial of order 8, the weighting factors and roots of the polynomial is given in Table C-1.

Table C-1

Weighting Factors and Roots of the 8-th Order Hermite Polynomial

i	Roots x_i	Weighting Factor H_i
1	.381,186,990,207	.661,147,012,558
2	1.157,193,712,447	.207,802,325,815
3	1.981,656,756,696	.017,077,983,007
4	2.930,637,420,570	.000,199,604,072
5	-2.930,637,420,570	.000,199,604,072
6	-1.981,656,756,696	.017,077,983,007
7	-1.157,193,712,447	.207,802,325,815
8	- .381,186,990,207	.661,147,012,558

Appendix C-2 Flowchart of the Main Program to calculate the Rate Data

Notations:- T_o = initial temperature (°K)
α = heating rate (°K/min)
t = time (min)
σ = standard deviation of the particle size distribution
2μ = wt. average size of particle
D_o = pre-exponential factor
E = activation energy
NOB = no. of data points
$\frac{dZ}{dt}$ = rate of desorption

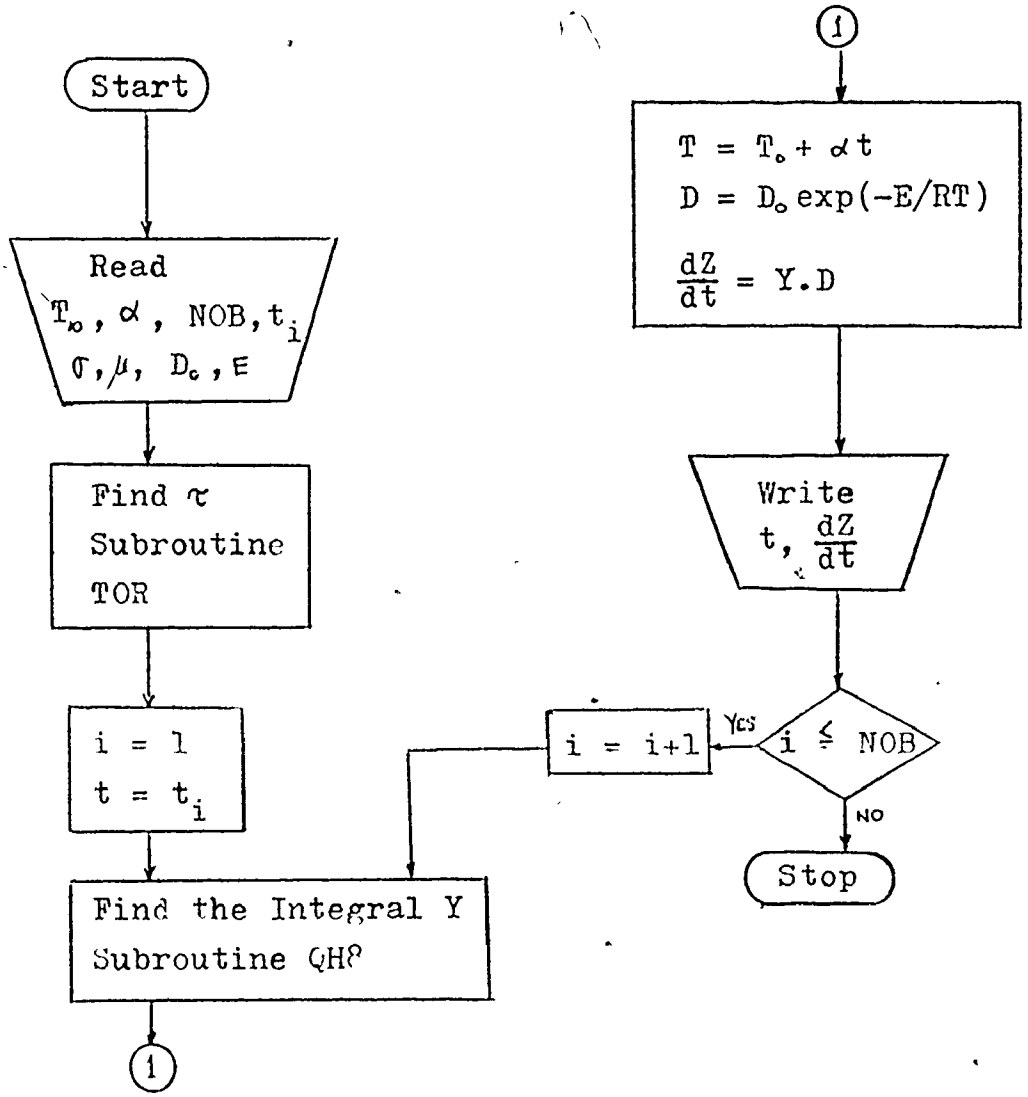

Appendix C-3

Computer Program Printout

```
      PROGRAM TST (INPUT,OUTPUT,TAPE5=INPUT,TAPE6=OUTPUT)
C     MODEL TO CALCULATE RATE OF DESORPTION
C     USING THE SERIES SOLUTION OF THE DIFFUSION EQUATION
C     DEFINITIONS
C     UM = HALF LENGTH OF THE CUBIC PARTICLE
C     SIG = STANDARD DEVIATION OF THE PARTICLE SIZE DISTRIBUTION
C     AF = HEATING RATE
C     TO = INITIAL TEMPERATURE
C     TM = TIME
C     TEM = TEMPERATURE
C     TAU = THE INTEGRAL OF DIFFUSIVITY WITH RESPECT TO TIME
C     E = EXPERIMENTAL RATE
C     DZ = CALCULATED RATE
C     DF1 = PREEXPONENTIAL FACTOR
C     ACTIVATION ENERGY FOR DIFFUSION
C     NOB = NUMBER OF DATA POINTS
C     FCT = THE FUNCTION TO CALCULATE THE INTEGRAL
C
      DIMENSION TM(30),DZ(30),TEM(30),TAU(30),AK1(30),E(30)
      COMMON TAU1,UM,SIG
      EXTERNAL FCT
      READ(K,17)TO,AF,DF1,E1,UM,SIG
   17 FORMAT(6F10.3)
      READ(5,12) NOB
   12 FORMAT(I5)
      DO 69 I=1,NOB
      READ(5,101) TM(I),E(I)
   69 CONTINUE
  101 FORMAT(2F10.3)
C
C     TO CALCULATE TAU
      CALL TOR ( DF1,E1,NOB,TO,AF,TM,TAU )
C
C     TO CALCULATE THE INTEGRAL Y AT EACH TAU
      DO 9 I=1,NOB
      TAU1 = TAU(I)
      CALL QHB(FCT,Y)
      TEM(I) = TO + AF*TM(I)
      AK1(I) = DF1*EXP(-E/(1.987*TEM(I)))
      DZ(I) = Y*AK1(I)/SQRT(3.1416)
      WRITE(6,102) TM(I), DZ(I)
    9 CONTINUE
  102 FORMAT(F10.2,E16.4,//)
      STOP
      END
```

FUNCTION FCT 73/73 OPT=2

```
      FUNCTION FCT(X)
      DIMENSION TM(1)
      COMMON /AA/TM/B3/AF,TO,UM,SIG,TAU1
      A = UM*EXP(1.4142*X*ALOG(SIG))
      S3 =0.0
      S4 = 0.0
      DO 7 N=1,20
      FN= N
      S1 = EXP(-(2.*FN-1.)**2*2.4674*TAU1/(A*A))
      S2 = EXP(-(2.*FN-1.)**2*2.4674*TAU1/(A*A))/(2.*FN-1.)**2
      S3 = S3 + S1
      S4 = S4 + S2
    7 CONTINUE
      R = S4-S4
      S = S3
      FCT = 3.9421*R*S/(A*A)
      RETURN
      END
```

```
      SUBROUTINE TOR ( AKO, E, NOB, TO, AF, TM, TORE )
      DIMENSION T(50),TORE(30),TM(30),Y(30)
      FCT(ARG) = 1.0/(ARG**2*EXP(ARG))
      R = 1.987
      YO = E/(R*TO)
      EPS = 0.01
      DEL = 0.01
      B=YO
      DO 90 I = 1, NOB
      Y(I) =  E/(R*(TO + AF*TM(I)) )
      A=Y(I)
      XO=A
      H=B-A
      T(1)=(H/2.)*(FCT(A)+FCT(B)  )
      N=1
    5 H=H/2.
      S=FCT(A)
      LIM=2**N-1
      DO 10 J=1,LIM
      X=XO+FLOAT(J)*H
   10 S=S+2.0*FCT(X)
      T(N+1)=(H/2.)*(S+FCT(B))
      F=(T(N+1)-T(N))/T(N)
      IF (ABS(F) - EPS) 60,60,15
   15 IF (H-DEL)25,25,20
   20 N=N+1
   22 GO TO 5
   25 NMAX = N
      N=1
   26 M=1
      K=N
   28 T(K)=(4.**M*T(K+1)-T(K))/(4.**M-1.)
      IF (K-1)40,40,30
   30 G =  (T(K)-T(K-1))/T(K-1)
      IF (ABS(G)-EPS) 50,50,35
   35 M=M+1
      K=K-1
      GO TO 28
   40 N=N+1
      IF (N-NMAX) 26,26,45
   45 DEL = DEL/2.
      GO TO 5
   50 WRITE(6,110) T(K)
      GO TO 65
   60 CONTINUE
   65 CONTINUE
  100 FORMAT(2F15.7,2F10.4)
  110 FORMAT(20H CONVERGED ROMBERG ELEMENT = ,  E15.6)
  111 FORMAT (2X,*CONVERGED TRAPEZOID SUM = *,E15.6)
      TORE(I) = T(N+1)*AKO*E/(AF*R)
   90 CONTINUE
      RETURN
      END
```

Appendix D-1 Rate Data for Nitrogen

Table D-1.1 N_2 Rate Data

(α = 3.19°C/min.)

Time (min)	Temperature (°C)	Z	$\frac{dZ}{dt} \times 10^2$ (min^{-1})
0	25	0	0
7.5	40.5	0	0
15.	63.	0	0
22.5	88.	.003	.015
30.0	112.	.007	.045
37.5	136.	.013	.120
45.	161.5	.031	.33
52.5	186.	.07	.66
60.	210.	.138	1.10
67.5	234.5	.240	1.48
75.	259.	.369	1.80
82.5	282.	.508	1.86
90.	307.	.65	1.74
97.5	330.	.768	1.31
105.	354.	.852	.9
112.5	377.	.908	.55
120.	401.	.943	.3
127.5	423.	.955	.14
135.	447.	.965	.10
142.5	470.	.973	.09

Table D-1.2 N_2 Rate Data

(α = 5.33°C/min.)

Time (min)	Temperature (°C)	Z	$\frac{dZ}{dt} \times 10^2$ (min^{-1})
0.	25	0	0
22.5	130.5	0	0
26.25	150.	.008	.21
30.	170.	.023	.46
33.75	190.	.052	.86
37.5	210.	.098	1.37
41.25	228.	.163	1.85
45.	247.5	.246	2.31
48.75	266.5	.342	2.63
52.5	286.5	.448	2.86
56.25	304.	.562	2.85
60.	323.	.668	2.54
63.75	342.5	.760	2.04
67.5	361.	.831	1.55
71.25	379.	.883	1.11
75.	397	.922	.74
78.75	416.	.945	.42
82.5	435.	.958	.23
86.25	454.	.968	.19
90.	472.	.977	.14
93.75	490.	.983	.12

Table D-1.3 N_2 Rate Data

($\alpha = 17^{\circ}C/min.$)

Time (min)	Temperature (°C)	Z	$\frac{dZ}{dt} \times 10^2$ (min^{-1})
8	145	.003	.22
9	162	.006	.44
10	180	.014	.85
11	197	.026	1.48
12	216	.047	2.38
13	233	.078	3.48
14	251	.122	4.66
15	263	.173	5.84
16	284	.240	6.96
17	301	.316	7.9
18	318	.404	8.62
19	336	.491	8.95
20	352	.582	8.73
21	368	.665	7.96
22	385	.740	6.87
23	402	.803	5.56
24	419	.855	4.26
25	435	.893	3.06
26	452	.918	1.94
27	468	.935	1.15
28	484	.945	.71
29	501	.951	.49

Table D-1.4 N_2 Rate Data

(α = 12.57 C/min.)

Time (min)	Temperature (C)	Z	$\frac{dZ}{dt} \times 10^2$ (min^{-1})
11	151	.002	.26
13	175	.013	.76
15	200	.040	1.71
17	225	.089	2.93
19	254	.162	4.27
21	280	.264	5.56
23	305	.389	6.39
25	330	.522	6.61
27	355	.656	6.16
29	380	.771	4.83
31	404	.853	3.33
33	429	.909	1.93
35	458	.940	.93
37	478	.956	.47
39	502	.964	.28
41	526	.970	.19
43	551	.973	.13

Appendix D-2 Rate Data for Carbon Dioxide

Table D-2.1 CO_2 (α = 6.86)

Time (min)	Temperature (°C)	Z	$\frac{dZ}{dt} \times 10^2$ (min^{-1})
10	84.	.0026	.16
12	97.	.0079	.36
14	110.	.020	.73
16	123.5	.042	1.32
18	137.	.078	2.05
20	151	.128	2.83
22	166.	.193	3.47
24	180.	.270	3.88
26	194.	.351	3.99
28	208.	.433	3.89
30	221.	.509	3.67
32.	235	.582	3.41
34	249	.649	3.06
36	262	.707	2.64
38	277	.757	2.13
40	290	.797	1.66
42	304	.828	1.25
44	317	.851	.93
46	331	.87	.75
48	344	.886	.63

Table D-2.2 CO_2 Rate Data

(α = 11° C/min.)

Time (min)	Temperature (°C)	Z	$\frac{dZ}{dt} \times 10^2$ (min^{-1})
8.	105.	.006	.38
10.	127	.021	1.06
12	150	.054	2.31
14	172	.119	3.94
16	195	.216	5.28
18	217	.330	5.83
20	239	.447	5.74
22	261	.560	5.10
24	283	.653	4.03
26	305	.723	2.83
28	326	.771	1.84
30	348	.803	1.29
32	369	.827	1.01
34	390	.850	.84
36	411	.864	.70

Table D-2.3 CO_2 Rate Data

(α = 14°C/min.)

Time (min.)	Temperature (°C)	Z	$\frac{dZ}{dt} \times 10^2$ (min^{-1})
7	115	.012	.77
8	129	.023	1.33
9	143	.041	2.25
10	157	.07	3.47
11	172	.111	4.84
12	186	.163	6.20
13	199	.236	7.27
14	213	.313	7.89
15	227	.393	8.07
16	241	.476	7.87
17	255	.553	7.20
18	269	.622	6.37
19	283	.682	5.33
20	297	.733	4.40
21	310	.773	3.44
22	325	.804	2.60
23	338	.829	2.0
24	351	.847	1.6
25	365	.861	1.33
26	379	.873	1.13
27	392	.886	.92

Table D-2.4 CO_2 Rate Data ϕ

(α = 17.02°C/min.)

Time (min)	Temperature (°C)	Z	$\frac{dZ}{dt} \times 10^2$ (min^{-1})
6	113	.002	.76
8	149	.020	2.84
10	185	.081	5.68
12	219	.193	7.24
14	255	.338	8.08
16	289	.509	7.74
18	324	.667	5.72
20	358	.778	3.28
22	391	.857	1.83
24	425	.887	1.33
26	458	.917	1.01
28	490	.939	.73
30	524	.956	.51

Appendix D-3 Rate Data for Argon

Table D-3.1 Ar (α = 16.83)

Time (min)	Temperature (°C)	Z	$\frac{dZ}{dt}$ X 10^2 (min^{-1})
10	172	.004	.27
12	207	.017	.93
14	241	.051	2.07
15	256	.078	2.72
16	276	.11	3.45
17	289	.15	4.28
18	310	.199	5.18
19	323	.256	5.97
20	344	.325	6.6
21	357	.393	6.9
22	374	.465	6.83
23	394	.53	6.23
24	411	.59	5.30
25	428	.64	4.13
26	445	.678	3.05
27	461	.705	2.25
28	479	.728	1.8
29	495	.745	1.56
30	512	.764	1.38
31	529	.775	1.13
32	546	.788	.75
33	562	.795	.48
34	579	.80	.36

Table D-3.2 Ar Rate Data

(α = 13.32°C/min.)

Time (min.)	Temperature (°C)	Z	$\frac{dZ}{dt} \times 10^2$ (min^{-1})
12	186.	.018	.87
14	213.5	.045	1.74
16	240.	.095	2.84
18	267.	.165	3.97
20	293.5	.255	4.98
22	320.	.369	5.92
24	347.	.495	6.34
26	373.5	.624	6.01
28	400.	.737	4.74
30	426.5	.814	3.60
32	453.	.866	1.96
34	480.	.903	1.45
36	506.5	.932	1.31
38	533.	.956	.81
40	559.	.968	.34

Table D-3.3 Ar Rate Data

(α = 10.87 °C/min.)

Time (min)	Temperature (°C)	Z	$\frac{dZ}{dt} \times 10^2$ (min^{-1})
3.75	118.	0	0
7.5	137.	0	0
11.25	168.	.005	.33
15.	220.	.038	1.11
18.75	240.	.103	2.18
22.5	273.	.203	3.08
26.25	301.	.343	4.3
30.	341.	.521	4.88
33.75	348.	.694	3.82
37.5	362.	.809	2.02
41.25	382.	.867	1.18
45.	401.	.911	1.04
48.75	426.	.942	.04
52.5	448.	.953	.02